Send Orders for Reprints to reprints@benthamscience.net

Current Pharmaceutical Design, XXXX, *XX,* 1-21

RESEARCH ARTICLE

A Nanophytomedicine Approach Including Tea Tree Essential Oil for Possible Dental Applications: *In vitro* and *In silico* Evaluations

Yasemin Budama-Kilinc[1,2,*], Nisanur Cakmakci[3,4], Serda Kecel-Gunduz[5], Şeyma Suyabatmaz[6], Sengul Alpay-Karaoglu[6], Pınar Yilmaz-Atali[4,7], Evren Algın Yapar[8,*] and Murat Kartal[9,10]

[1]*Department of Bioengineering, Faculty of Chemistry and Metallurgy, Yildiz Technical University, Istanbul, 34220, Türkiye;* [2]*Health Biotechnology Joint Research and Application Center of Excellence, Istanbul, 34220, Türkiye;* [3]*Department of Biotechnology, Graduate School of Natural and Applied Science, Yildiz Technical University, Istanbul, 34220, Türkiye;* [4]*Umbrella Biotechnology Inc. Co., Teknopark Istanbul, Istanbul, 34906, Türkiye;* [5]*Physics Department, Faculty of Science, Istanbul University, Istanbul, 34134, Türkiye;* [6]*Department of Biology, Recep Tayyip Erdogan University, Rize, 53100, Türkiye;* [7]*Department of Restorative Dentistry, Faculty of Dentistry, Marmara University, Istanbul, 34854, Türkiye;* [8]*Department of Pharmaceutical Technology, Faculty of Pharmacy, Sivas Cumhuriyet University, Sivas, Türkiye;* [9]*Faculty of Pharmacy, Bezmialem Vakif University, Istanbul, 34093, Türkiye;* [10]*Phytotheraphy Research and Application Center, Bezmialem Vakıf University, Istanbul, Türkiye*

ARTICLE HISTORY

Received: April 16, 2025
Accepted: August 05, 2025

DOI:
10.2174/0113816128401462251128162600

Abstract: ***Introduction:*** Tea tree essential oil (TTO) incorporated polylactic-co-glycolic acid (PLGA) nanoparticulate powder form was aimed to desined that can be applied with water and is effective against oral pathogens to prevent caries, and that is able to provide a long-lasting oral antiseptic effect.

Methods: TTO-PLGA nanoparticles (TTO-NPs) was synthesized by single emulsion technique; average particle size, PdI value and zeta potential was measured by Zetasizer; TTO-PLGA interactions were investigated by FTIR, and morphological analysis was performed by TEM analysis. Phytoactive release and performans tests were carried out with *in vitro* dissolution and DNA binding-cleavage tests while antimicrobial performance was investigated by Ames-Salmonella assay, susceptibility test, *in silico* Molecular Docking and Molecular Dynamics studies.

Results: TTO-NPs had an average particle size of 221.6 nm, a PdI of 0.103, and a zeta potential of -5.22 mV, 59.25% encapsulation efficiency and 25.65%. loading capacity. At the end of 5 h and 72 h the TTO release was 33.34±2.17% and 97.61±3.91% respectively. TTO-NPs were not mutagenic and were effective on investigated four cariogenic bacteria. The binding interactions of terpinen-4-ol, the main component of TTO, with *Streptococcus muta*ns and *Lactobacillus casei* were revealed with enzyme-active-site-key residues.

Discussion: *In vitro* and *in silico* studies confirmed that TTO-NPs were non-mutagenic and exhibited strong antimicrobial activity against dental caries-causing bacteria like *Streptococcus mutans* and *Lactobacillus casei*.

Conclusion: In conclusion, TTO-NPs, which can be used as a mouthwash or powder, represent a promising solution for reducing oral pathogens, meriting further *in vivo* and clinical evaluations.

Keywords: Nanophytomedicine, tea tree oil, polylactic-co-glycolic acid, mouth pathogens, antimicrobial performance, *in silico* evaluation, molecular docking, molecular dynamics.

1. INTRODUCTION

Tooth decay is a widespread disease that affects a significant portion of the global population. The worldwide distribution of dental caries prevalence has been non-homogeneous for many years. Developed countries are reducing the prevalence of dental caries in their populations by implementing public health strategies focused on prevention. In contrast, the prevalence of dental caries remains high in undeveloped and developing countries, where socioeconomic status is low, access to oral and dental health services is limited, and preventive dentistry practices are not adopted [1]. According to data from The Turkish Statistical Institute, oral and dental health problems are among the top five diseases in the 0-6 age group (6.4%) and in third place with 14.2% in the 7-14 age group. As previously documented, dental caries has been identified as the most prevalent pathology during general health screenings conducted among school-age children in Türkiye. A body of research has been conducted on a global scale to determine the prevalence of dental caries at the age of five years. The prevalence was found to be 53.9% in Brazil, 16.5% in Greece, and 44.4% in India. In 12-year-old children, the prevalence of dental caries was reported as 22.3% in India, 56% in Lao, 43.1% in Italy, 62% in Iraq, and 45.7% in Germany. The prevalence of dental caries in children aged 15 years in the Southeast region of Macedonia was 82.75%, 82% in India, 47.2% in South Africa, and 92.9% in Lithuania [1, 2].

*Address correspondence to these authors at the Department of Bioengineering, Faculty of Chemistry and Metallurgy, Yildiz Technical University, Istanbul, 34220, Türkiye; Health Biotechnology Joint Research and Application Center of Excellence, Istanbul, 34220, Türkiye; E-mail: yaseminbudama@gmail.com (Y.B-K.); Department of Pharmaceutical Technology, Faculty of Pharmacy, Sivas Cumhuriyet University, Sivas, Türkiye; E-mail: evren.yapar@yahoo.com (E.A.Y.)

Dental caries are caused by several reasons, including bacteria buildup and microbial plaque development [2, 3]. *Streptococcus mutans Lactobacillus casei, Lactobacillus acidophilus* and *Scardovia wiggsiae* are the bacteria that have a role in the formation of dental caries [4, 5]. The increased prevalence of dental caries and associated disorders, particularly in emerging nations, in addition to antibiotic-resistant pathogenic microorganisms and undesirable effects of frequently used antibacterial substances, such as amine fluorides, chlorhexidine, and cetylpyridinium chloride, means that effective oral care product alternatives need to be developed [6-9]. In line with studies on nanomaterials that have proved their antibacterial effectiveness, many nanomaterials such as zinc oxide, titanium oxide, copper oxide, graphene, silver, silica, and also chitosan were studied to control dental biofilm formation [10-13]. Additionally, researches showed that nanoparticles have a specific affinity to tooth surfaces, which present a significant advantage to prevent the adhesion of bacteria to the tooth sufaces [14-18]. The antibacterial effectiveness of essential oils on mouth pathogens is known and they have been used in various mouth care products especially in mouthwashes [19, 20]. Particularly, natural sources that contain polyphenols are preferable, and they have also been used in traditional medicines [21]. Between those, tea tree oil is widely used in many personal care products, including oral care ones, especially in Europe and America, due to its antimicrobial and anti-inflammatory effects. However, its oral use is limited due to its toxicity [22, 23]. There have been studies conducted on tea tree oil dental applications [24, 25] and proved antimicrobial effectiveness of the oral mouthwashes containing 0.2%-0.5% tea tree oil may limit dental plaque accumulation and a periodental gel containing 5% tea tree oil may help to treat periodontitis [24]. Polymeric encapsulation of bioactives has present benefits including the increase of the stability of many phytobioactives. And in case of formation of polymeric particles in nanoparticular sizes the ability of adhesion and penetration of those have been increased [26-29]. The development of low-toxicity, antibacterial, and bad breath prevention alternative oral care products has been achieved through the use of nanoparticles prepared with tea tree extract. These products have been formulated to ensure optimal oral hygiene in cases where mechanical cleaning is inadequate. In addition to these benefits they also provide to decrease the loaded efficient doses of phytobioactives such as essential oils resulted as decrease in toxicity especially by using biocompatible and biodegradable polymers such as polylactic-co-glycolic acid (PLGA) [30, 31]. In the light of the studies showed the effectiveness of the tea tree oil on oral pathogens and the benefits of phytoactives loaded nanoparticular delivery in the treatment, in this study, it was aimed; to synthesis of tea tree oil (TTO) combined PLGA nanoparticles (TTO-NPs); to evaluate their effectiveness by using *in vitro* and *in silico* antimicrobial effectiveness tests in addition to safety evaluation by using DNA cleavage-binding studies and genotoxicity determined by the Ames/ Salmonella test. The difference of this study from the existing ones is to create a nanoparticle powder form that can be mixed with tooth powder or water during use, different from the classical tea tree oil-containing dosage forms and has a longer lasting effect than immediate action mouthwashes *etc*. In the first step the phytochemical composition of tea tree oil (essential oil of *Melaleuca linariifolia var. alternifolia* Maiden & Betche) was determined by using Gas Chromatography coupled with Flame Ionization Dedector/ Mass Spectrometry (GC-FID/MS) analysis and to determine tea tree oil concentration in various media analytical calibration was created by using UV-Vis spectrophotometer. In the second step TTO combined PLGA nanoparticles was prepared by using single emulsion technique, the encapsulation efficency was calculated and *in vitro* TTO release from TTO-NPs was studied. The physicochemical characterization of TTO-NPs was performed by determination of average particle size, PdI value and zeta potential, TTO and PLGA interactions by Fourier Transform Infrared Spectroscopy (FTIR) analysis, investigation of their surface morphology by using Transmission electron microscopy (TEM) analysis. In the third step *in vitro* antibacterial effectiveness of the TTO-NPs, which were in solid powder form were investigated by DNA Binding Assay, DNA Cleavage Assay, antimicrobial susceptibility test and *in silico* Molecular Docking (docking-MD) and Molecular Dynamics (dynamics-MD) studies. In the fourth step safety of TTO-NPs was investigated by Ames/Salmonella Test.

2. MATERIALS AND METHODS

2.1. Materials

Australian Tea Tree (*Melaleuca alternifolia*) oil from FitoBio (Istanbul-Türkiye) series MAEO0722 was used that conforms to the ISO standard. Polyvinyl alcohol (PVA) (CAS no. 9002-89-5), PLGA (CAS no. 26780-50-7), calf thymus DNA (CT-DNA), ethidium bromide and dichloromethane (DCM) (CAS no. 75-09-2) were purchased from Sigma Aldrich. Sodium chloride (NaCl), sodium hydroxide (NaOH), Tris base hydrochloric acid (Tris-HCl) and ethylene diamine tetra acetic acid (EDTA) were purchased from Merck Millipore (Burlington, MA, USA). Graphical abstract was created with BioRender.com. Homogenizer (Bandelin HD, Berlin, Germany), lyophilizer (Biobase, Shandong, China), UV-Vis spectrophotometer (Shimadzu, Kyoto, Japan), centrifuge (Hettich-Universal 320R, Tuttlingen, Germany) and Zeta Sizer Nano ZS (Malvern Instruments, Malvern, UK) were used.

2.2. Metods

2.2.1. GC-FID/MS Analysis of Essential Oil

Solutions of 10% (v/v) essential oils in n-hexane were subjected to GC-FID/MS analysis. An Agilent 7890B GC-FID (Santa Clara, CA, USA) coupled with an Agilent 5977E electron impact mass spectrometer (Santa Clara, CA, USA) *via* a two-way capillary splitter was utilized to identify and quantify essential oil components. Analyses were performed in triplicate and using a similar method in our previous work [32].

2.2.2. Calibration Curve of the TTO

TTO solution was prepared at seven different concentrations (200; 100; 50; 25; 12.5; 6.25; 3.125 µg/mL). Then, a calibration curve was created by measuring the absorbance values of each concentration using a UV-Vis spectrophotometer. The calibration curve was used to determine the amount of TTO encapsulated with PLGA and the amount of TTO released in the *in vitro* release experiment.

2.2.3. Preparation of the TTO-NPs

A single emulsion technique was used to synthesize TTO-NPs [32] Briefly, 1% PLGA solution was prepared with DCM and mixed with 40 mg of TTO. TTO-NPs mixture was added dropwise into a 5% PVA solution with the help of an insulin injector. This mixture was sonicated for 2 minutes under 70 W energy. The homogenized solution was stirred for 16 hours on a magnetic stirrer, and the solvent (DCM) was evaporated. After evaporation, washing with ultrapure water was performed by applying centrifugation (three times, each time for 40 min) at 8000 rpm to remove the solvent from the nanoparticle solution. Blank NPs were also synthesized using the same procedure without TTO added. The prepared nanoparticle solutions were dried by lyophilization.

2.2.4. Average Particle Size, Polydispersity Index (PdI) and Zeta Potential Analyses of the TTO-NPs

The average particle size, PDI value, and zeta potential of solid TTO-NPs were evaluated using a ZetaSizerNano ZS (Malvern Instruments, UK) instrument equipped with a 4.0 mV He-Ne laser (633 nm) operating at 25°C by dynamic light scattering. Lyophilized

TTO-NPs were homogeneously dissolved with distilled water (1:10 ratio), and then measured in triplicate.

2.2.5. Determination of the Encapsulation Efficiency and Loading Capacity

The centrifugation process used to make TTO-NPs solid particles allowed for measuring the TTO concentration in the supernatant. Utilizing the absorbance measurement from the UV-Vis spectrometer. The total TTO content was calculated from the curve equation. The encapsulation efficiency (EE) was calculated using Equation (1). The loading capacity (LC) was also calculated using Equation (2).

$$\text{EE \%} = \frac{Total\ amount\ of\ loaded\ TTO}{Initial\ amount\ of\ the\ TTO} \times 100\% \quad \text{Eq. (1)}$$

$$\text{LC \%} = \frac{Total\ amount\ of\ loaded\ TTO}{NPs\ after\ freeze\ drying - Weight\ of\ the\ TTO} \times 100\% \quad \text{Eq. (2)}$$

2.2.6. Investigation of In vitro Release Profile of TTO-NPs Powder

TTO-NPs, which were in solid powder form, were dissolved in distilled water and inserted into the dialysis capsule to assess the release profile of TTO. The release medium was composed of 40% ethanol and 60% phosphate buffer (pH 7.4). At room temperature and 120 rpm, capsules were incubated in a horizontal shaking water bath. Samples taken from the release medium at the specified periods were analyzed with UV-Vis spectrometry. The release was calculated using Equation (3) [33, 34].

$$\text{Release \%} = \frac{\boldsymbol{Released\ TTO}}{\boldsymbol{Total\ TTO}} \times 100\% \quad \text{Eq. (3)}$$

2.2.7. FT-IR Spectroscopy Analysis

Blank NPs and TTO-NPs and FTIR characterizations of TTO were performed in the 4000-400 cm^{-1} wavenumber region using the Jasco 6300E FT-IR spectrometer with diamond ATR unit.

2.2.8. TEM Analysis of the TTO-NPs

Morphological analysis of TTO-NPs in solid powder form was performed using TEM (JEOL JEM-1400 Plus). 3 mg of lyophilized nanoparticle sample was transferred into water and sonicated in an ultrasound bath for 45 minutes. Dry samples were dispersed in isopropyl alcohol, and 1 µL of the solution was taken and dropped onto a carbon film-supported copper grid. The solvent was analyzed after evaporation. TEM images were taken by working with 80 kV voltage.

2.2.9. DNA Binding Assay

Substances that bind to and cut DNA are essential for bacterial and cancer diseases. The most popularly straightforward way for illuminating the conformational changes of biomacromolecules in the presence of small molecules is a UV-visible absorption spectrum [35]. The UV-Vis absorption titration method was used to conduct a DNA binding assay at room temperature in a Tris-HCl/NaCl buffer (pH 7.2). The experiment was carried out by adding increasing amounts of CT-DNA to seven different concentrations from 10 µM to 75 µM and a constant amount of TTO concentration. To prevent CT-DNA from absorbing itself, equal volumes of CT-DNA were added to the TTO-containing solution and the reference solution before measuring the absorption. TTO-DNA solutions were incubated for 5 minutes at room temperature, and their absorption spectra were recorded [33].

2.2.10. DNA Cleavage Assay

The ability of TTO and TTO-NPs powder to cleave DNA was observed using the agarose gel electrophoresis method. Using pBR322 DNA, DNA cleavage characteristics of TTO and TTO-NPs were examined both in the presence of an oxidizing agent (H_2O_2) and without an oxidizing agent (hydrolytic cleavage). EcoRI restriction enzyme was used as the positive control, and a 1 kb DNA ladder was used as the marker. Solutions were prepared separately for TTO and TTO-NPs by adding pBR322 DNA (0.1 µg/µL) to Tris-HCl buffer (10 M, pH: 7.2) of water/H_2O_2, and the prepared solutions were left for 3 h incubation at 37°C. Following the incubation, samples were run in TBE (Tris-Boric acid-EDTA, pH: 8.0) buffer for 1 hour at 60 V. Finally, UV light was used to see the bands formed due to the execution.

2.2.11. Ames/Salmonella Test

A biological experiment known as the Ames test is used to evaluate the mutagenic potential of chemical substances such as medications, dyes, reagents, cosmetics, pesticides, or wastes. Bacteria are used to determine whether specific sample results in DNA mutations in the test organism. *Salmonella typhimurium* TA98 and TA100 strains are the best-standardized strains against frameshift and base pair substitution mutations [36]. Therefore, *Salmonella typhimurium* TA98 and TA100 strains were used in this study. TTO and TTO-NPs powder form were utilized at four different concentrations following the findings of the *in vitro* release investigation. The doses that allowed these strains to synthesize histidine were tried to be determined. The number of colonies that could synthesize histidine was compared to the negative control group to assess the outcomes. The sample that caused the colonies shown in the negative control to multiply two-fold was deemed mutagenic. It was thought to have a weak mutagenic effect when the quantity of returned bacteria increased in a dose-dependent manner.

2.2.12. Antimicrobial Susceptibility Test

Antimicrobial activity for empty NPs, TTO-NPs, and TTO was performed against *Lactobacillus casei, Lactobacillus acidophilus, Streptococcus mutans, Streptococcus wiggsiae* bacteria using the agar well diffusion method. MRS agar and broth (Merck) media were used for *Lactobacillus casei* and *Lactobacillus acidophilus* strains. For *Streptococcus mutans* and *Streptococcus wiggsiae*, 5-7% human blood Brain Heart Infusion agar (BHIA) and bloodless BHI broth were used.

Bacteria were resuscitated on appropriate agar medium for three days at 37°C, and in the microaerophilic medium. Bacterial suspensions of McFarland, 0.5 turbidities from fresh cultures were prepared in appropriate liquid media. Smears were applied using sterile swab sticks under sterile circumstances to the appropriate agar medium surfaces. The plate surface needs 30 minutes to dry. After waiting for drying procedure, wells with a diameter of 6 mm were opened with 2 cm spacing. Three replicates were tested by dropping 100 µL of TTO, blank NPs and TTO-NPs into each well. Three days were devoted to growing the cultures at 37°C in a microaerophilic medium. After incubation, the diameters of the non-growth zones around the wells were measured with the help of a ruler and evaluated as the inhibition zone diameter. Since *Streptococcus mutans* and *Streptococcus wiggsiae* were tested on BHIA, the diameters of the particles' non-growth zones were determined with a ruler's help.

2.2.13. In silico Analysis

In silico analysis was carried out with docking and dynamics-MD studies. The association of the antibacterial activity in TTO with its chemical composition rich in terpinen-4-ol, and its antibacterial activity against *Lactobacillus casei*, and *Streptococcus mutans* bacteria were also investigated using *in silico* methods. Terpinen-4-ol has antifungal and antibacterial properties and is the most abundant major active ingredient among

the complex mixtures of compounds in TTO. Therefore, Terpinen-4-ol was chosen as the active ligand. The three-dimensional structure of this ligand, which has a molecular formula of $C_{10}H_{18}O$ and is also known as 4-Carvomenthenol, was obtained from Pubchem [37] site, and its optimized geometric structure was used in both Docking and MD analyzes. *Streptococcus mutans*, the main bacterium responsible for dental caries, and *Lactobacillus casei*, which supports the formation of dental caries, were preferred as possible receptor structures to reveal the antibacterial activity. The crystal structure of glucan-sucrase from the dental caries pathogen *Streptococcus mutans* (PDB ID: 3AIC) [38] and the crystal structures of *Escherichia coli* and *Lactobacillus casei* dihydrofolate reductase (PDB ID: 1BZF) [39] were taken from the protein data bank [40]. For molecular docking analysis, using the "receptor preparation wizard" in the Schrödinger Glide module [41, 42], all other molecular structures, such as water and ions in the structure, were removed, and polar hydrogen atoms were added to the receptors. The bond patterns were determined, the charges were adapted by PROPKA [43] at neutral pH, and the heavy atoms were approximated by choosing the 0.3 Å RMSD value of the selected receptors. They were optimized by the OPLS3 force field [44]. In addition, by using the OPLS force field with the "LigPrep" tool in the Glide module of this program, the conformers of different geometries of the terpinen-4-ol ligand, which is the main active ingredient in the TTO, were obtained at neutral pH and all these conformers were used for docking analysis. Grids were created to determine the active binding sites of the receptors. By applying molecular docking analysis after the grid process, the binding affinities, binding sites, and binding mechanisms of the dockings process were examined, and the inhibition efficiencies of *Streptococcus mutans* and *Lactobacillus casei* were compared among themselves. Desmond simulation module of the same package program was preferred for dynamics-MD simulations [45, 46]. Ligand-receptor complexes, which achieved the most stable binding obtained in the docking analysis results, were placed in a cubic box containing the TIP3P water molecule model, and Na^+ and Cl^- ions were added to the system to neutralize the net charge of the system. MD simulations were performed for 50 ns after the NPT ensemble, followed by all systems to hold pressure (1 bar) and temperature (300ºK). The calculated root mean square deviation (RMSD) and the root-mean-square fluctuations (RMSF) of the MD trajectories provided an analysis of ligad-reseptors complexes. Reseptors-ligand interactions were also identified by the contact times and contact zones.

2.2.14. Statistical Analysis

Mutagenic activity data were subjected to analysis of variance (ANOVA) followed by Tukey's test with Statitix 9.0 Analytical Software 2008 for Windows (USA). Differences at $p<0.05$ were considered significant. Antimicrobial susceptibility test results were subjected to Student T test. Differences at $p<0.05$ level were considered significant.

3. RESULTS

3.1. GC-FID/MS Analysis of Essential Oil

A total of eleven compounds in TTO were detected and quantified. Table **1** presents the constituents in terms of the retention indices order. The components of TTO were found to be 45.476% terpinen-4-ol as the major compound, 22.039% γ-terpinene, and 9.748 % α-terpinene respectively.

3.2. Analysis of Average Particle Size, PdI, and Zeta Potential

The average particle size, PdI, and zeta potential of TTO-NPs and blank NPs were determined using DLS, an extensively utilized technique. It was found that the average particle size of the empty NPs was 196.4 nm, the PdI was 0.124, and the zeta potential was -6.08 mV, as shown in Figs. (**1a** and **b**), respectively. The average particle size of TTO-NPs was 221.6 nm, the PdI value was 0.103, and the zeta potential value was -5.22 mV (Figs. **2a** and **b**, respectively).

3.3. Determination of the Encapsulation Efficiency and Loading Capacity

The calibration curve (Fig. **3**) of TTO was used to assess the encapsulation efficiency and the loading capacity of the TTO-NPs. The encapsulation efficiency and the loading capacity of TTO-NPs were determined *via* Equation 1 and Equation 2 as 88.57% and 62%, respectively.

Table 1. Composition of TTO (*Melaleuca alternifolia* leaf essential oil).

No.	Compound	R.T (min)	$R.I^L$	$R.I^C$	Amount (%)
1	*α*-Pinene	6.966	1032	1028	3.865
2	*β*-Pinene	9.524	1118	1115	0.235
3	Sabinene	10.001	1132	1129	0.174
4	*α*-Terpinene	13.007	1186	1193	9.748
5	Limonene	14.169	1203	1207	2.571
6	1,8-Cineole	14.836	1214	1216	2.237
7	*γ*-Terpinene	17.759	1255	1261	22.039
8	*p*-Cymene	19.632	1280	1276	5.161
9	*α*-Terpinolene	20.487	1290	1287	2.801
10	Terpinen-4-ol	43.468	1610	1618	45.476
11	*α*-Terpineol	49.091	1707	1711	5.680
Total Identified					99.578
Monoterpenes (1-5, 7-9)					46.185
Oxygenated Monoterpenes (6, 10, 11)					53.393

Note: R.T; Retention time (min), $R.I^L$; Retention indices derived from literature and NIST webbook database, $R.I^C$; Calculated retention indices.

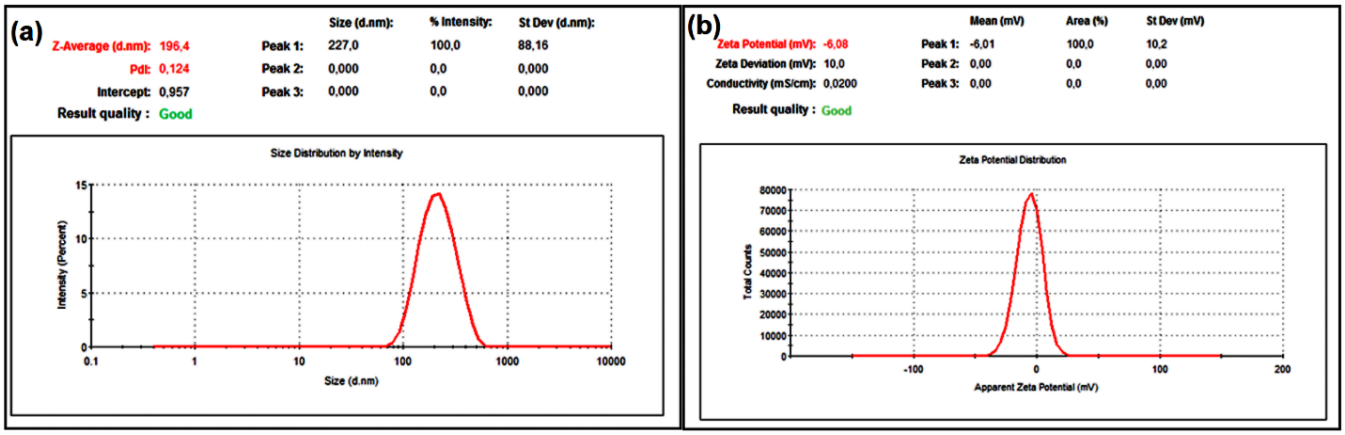

Fig. (1). DLS analysis of the blank NPs: (**a**) Average particle size, and (**b**) Zeta potential graphs. (*A higher resolution/colour version of this figure is available in the electronic copy of the article*).

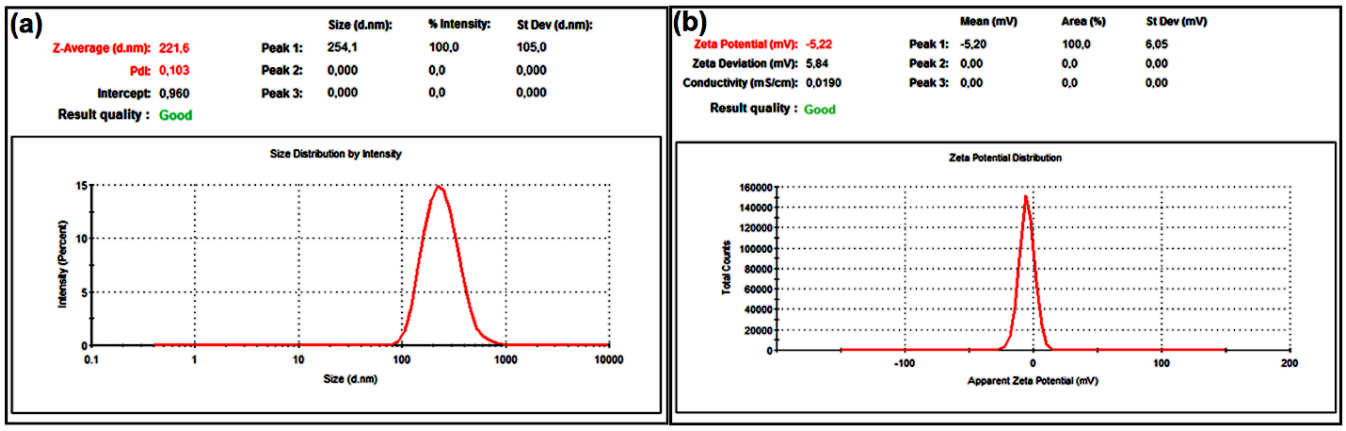

Fig. (2). DLS analysis of the TTO-NPs: (**a**) Average particle size, and (**b**) Zeta potential graphs. (*A higher resolution/colour version of this figure is available in the electronic copy of the article*).

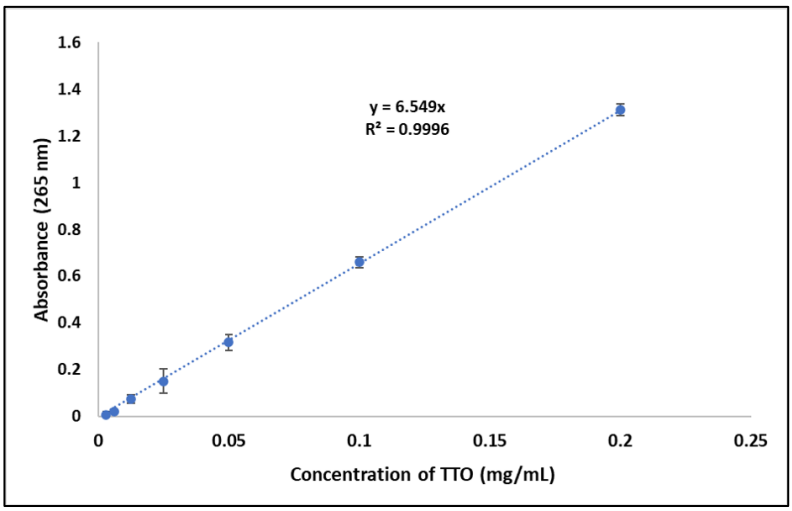

Fig. (3). Calibration curve of the TTO. (*A higher resolution/colour version of this figure is available in the electronic copy of the article*).

The spectrophotometric method was used to generate the calibration curve of TTO. Analysis was performed in PBS solution containing 3% Tween 80 using the method used by Ge *et al*. [47]. The peak from terpinen-4-ol at 265 nm was obtained for consecutive TTO concentrations. A calibration curve was created with the concentration values corresponding to the obtained absorbance values.

3.4. *In vitro* Release Profile of the TTO

The release profile of the TTO-NPs was assessed as a function of time. The release graph was plotted with time values and concentration values on the x-axis and y-axis, respectively. *In vitro* release results of TTO-NPs are given in Fig. (**4**). The result showed that at the end of the first 5 hours, 33.34%±2.17 of TTO was

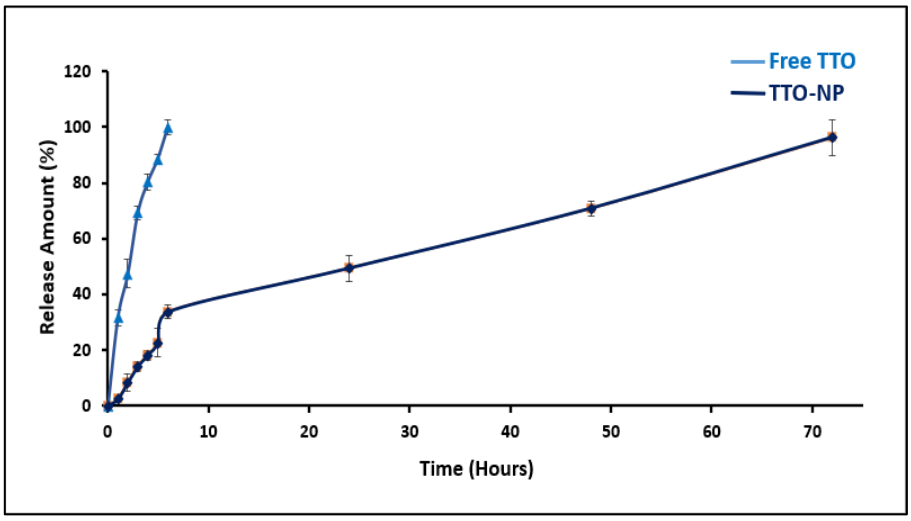

Fig. (4). *In vitro* release graph of TTO and TTO-NPs. (*A higher resolution/colour version of this figure is available in the electronic copy of the article*).

released in the sixth hour, and 97.61%±3.91 of TTO was released from TTO-NPs in the 72th hour.

3.5. FT-IR Spectroscopy Analysis

ATR-FTIR spectra spectra for blank NPs, TTO-NPs, and TTO were captured in three distinct areas (Fig. **5**). It is thought that the broad band observed in the spectrum between 3400 cm^{-1} and 3300 cm^{-1} is mainly due to the OH contribution of molecules such as terpinen-4-ol and α-terpineol in TTO. The peaks of TTO at 2960 cm^{-1}, 2915 cm^{-1}, 2877 cm^{-1} were observed in TTO-NPs at 2938 cm^{-1} and 2915 cm^{-1}. This region corresponds to the C-Hs found in the TTO to the stretching vibrations caused by the presence of -C-H bonds in almost all the components in the TTO (Fig. **5a**). The peak at 1641 cm^{-1} for TTO and TTO-NP spectra was attributed to C=C stretching. The C-H bending vibrations in compounds like terpinen-4-ol contributed to the formation of sharp peaks at 1444 cm^{-1} in the TTO spectrum in Fig. (**5b**). Also, it is thought that the alkaloid C-O bonds in these compounds contributed to a sharp peak at 1068 cm^{-1}. The C-O bond present in the TTO spectrum contributes to the sharp peak of high intensity at 1026 cm^{-1}. The region between 948 cm^{-1} and 721 cm^{-1} corresponds to =C-H bending vibrations of the compounds in the TTO in Fig. (**5c**). The peak observed at 924 cm^{-1} in TTO was not observed in TTO-NPs. The presence of TTO-related peaks in the spectrum of TTO-NPs showed that TTO was present in the structure of TTO-NPs, and the all peaks observed for TTO correspond [48]. Figure 5 illustrates the spectra of TTO, TTO-NPs, and blank NP, allowing for an in-depth exploration of their unique peaks. In (a), the expansive 4000-2400 cm^{-1}region, (b) the 1800-1000 cm^{-1} region, and (c) the 1100-500 cm^{-1} region.

3.6. TEM Micrograph of the TTO-NPs

TEM analysis is an imaging method that provides a better understanding of the actual geometric size of nanoparticles and information about their morphology [49]. In our study, the morphology analysis of TTO-NPs was performed by using TEM. As seen in Fig. (**6**), the nanoparticles were dispersed and the TTO-NPs were spherical shapes and smooth surfaces. However, a slight aggregation tendency was observed in some of the particles.

3.7. DNA Binding Assay

The interaction of TTO with DNA was determined by UV-Vis spectroscopy using CT-DNA. The TTO spectra were recorded by adding seven different increasing concentrations of varying CT-DNA (Fig. **7**). As seen from the figure, when CT-DNA was added successively, 46.5% hypochromism at 236.40 nm (indicated by the black arrow) and a red shift of 9 nm (indicated by the red arrow) were observed in the UV-Vis absorption of TTO.

3.8. DNA Cleavage Assay

The ability of TTO-NPs and TTO to fragment DNA was evaluated using the agarose gel electrophoresis method. It was visualized under UV light. Hydrolytic activity was not observed in the electrophoresis image of TTO-NPs and TTO, as seen in Fig. (**8**). In Fig. (**9**), it was observed that oxidative activity was caused by the direct interaction of TTO with DNA, as indicated in the electrophoresis images of TTO-NPs and TTO. TTO-NPs did not react with DNA resulted in no activity being seen.

3.9. Ames/Salmonella Test

In our study, the mutagenicity of TTO and TTO-NPs was evaluated with the Ames test. In experiments using TA98 and TA100 strains, results were evaluated using positive, negative, and spontaneous controls. The mutagenicity results of TTO and TTO-NPs were given in Tables **2** and **3**, respectively.

3.10. Antimicrobial Susceptibility Test

Antibacterial activity of blank NPs, TTO-NPs, and TTO was performed *via* agar well diffusion method against four different bacteria, *Lactobacillus casei, Lactobacillus acidophilus, Streptococcus mutans* and *Scardovia wiggsiae*. For all bacterial species, the inhibition zone diameter of the blank NPs group was measured as 0 mm. This finding statistically confirms that the observed antimicrobial activity is directly attributable to the tested TTO and TTO-NP substances, and that the nanoparticle matrix alone does not exhibit any antimicrobial effect. On the other hand, it was determined that bacteria were very sensitive to TTO; similarly, TTO-NPs were found to be effective on these bacteria (Table **4**).

3.11. *In silico* Analysis

3.11.1. Molecular Docking

Molecular docking analysis was performed using *Streptococcus mutans* (PDB ID: 3AIC) and *Lactobacillus casei* dihydrofolate reductase (PDB ID: 1BZF) receptors to predict the

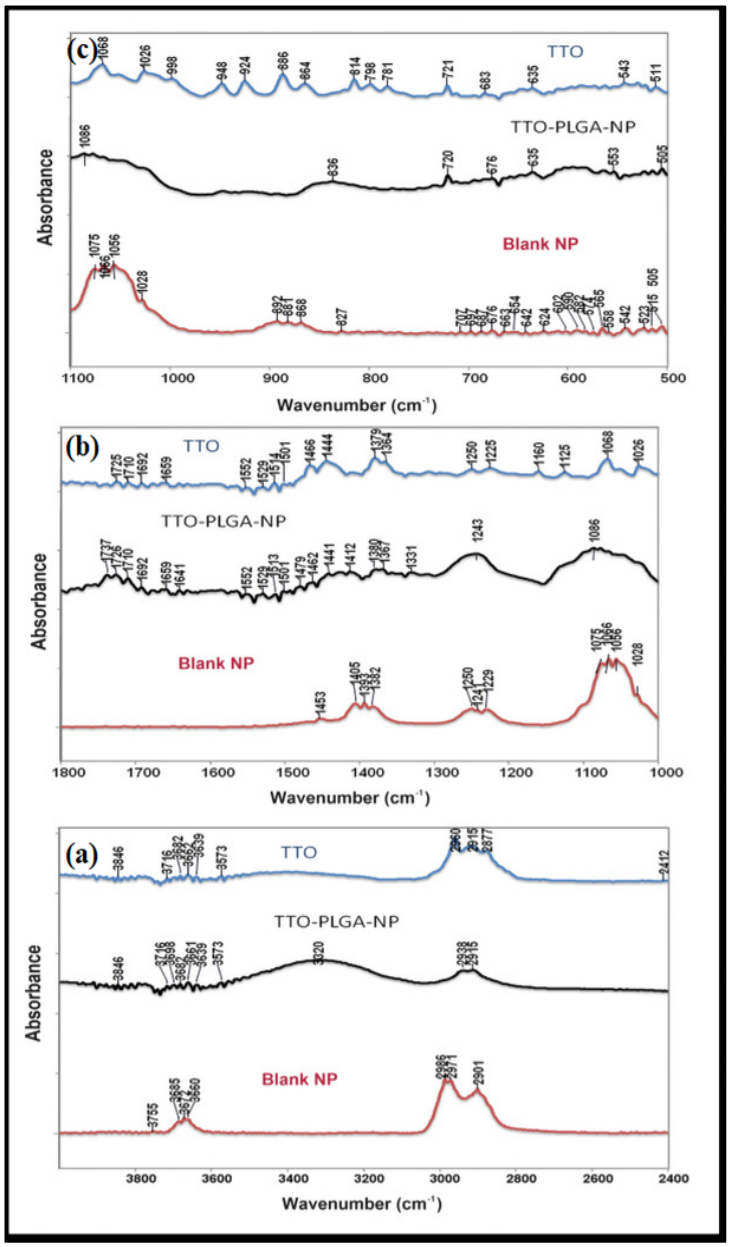

Fig. (5). Attenuated comparative total reflectance spectra of TTO, TTO-NPs, and blank NP are superimposed for a clearer view of the peaks. (**a**) shows the 4000-2400 cm^{-1} region, (**b**) the 1800-1000 cm^{-1} region, and (**c**) the 1100-500 cm^{-1} region. (*A higher resolution/colour version of this figure is available in the electronic copy of the article*).

Table 2. Genotoxicity results of TTO.

Treatment	Concentrations (mg/mL)	Number of Revertant Colony/Plate	
		TA98 Mean±SD	TA100 Mean±SD
TTO	0.10	170.00 ± 2.00*	199.33 ± 26.01
	0.205	148.33 ± 3.79*	366.67 ± 76.38*
	0.40	2.67 ± 2.08*	5.00 ± 3.00*
	0.80	4.00 ± 2.00*	3.67 ± 0.58*
Positive Control (NPD)	10^{-2}	947.67 ± 9.29*	-
Positive Control (NaN_3)	10^{-3}	-	1242.00 ± 73.12*
Negative Control (Water)	-	34.33 ± 2.08	165.00 ± 3.00*
Spontaneous Control	-	20.33 ± 2.08*	180.33 ± 41.50

Note: Asterisks (*) show differences in mean revertant colony numbers between the application and negative control groups that are significant at the level of $p<0.05$ (Tukey test).

Table 3. Genotoxicity results of TTO-NPs.

Treatment	Concentrations (mg/mL)	Number of Revertant Colony/Plate	
		TA98 Mean±SD	TA100 Mean±SD
TTO-NPs	0.125	24.67 ± 2.52	210.00 ± 10.00
	0.25	21.33 ± 2.08	178.00 ± 8.00
	0.50	20.67 ± 2.08	159.33 ± 34.93
	1.00	21.33 ± 3.06	150.00 ± 10.00
Positive Control (NPD)	10^{-2}	947.67 ± 9.29*	-
Positive Control (NaN_3)	10^{-3}	-	1242.00 ± 73.12*
Negative Control (Water)	-	20.33 ± 2.52	146.00 ± 6.00
Spontaneous Control	-	20.33 ± 2.08	180.33 ± 41.50

Note: Asterisks (*) show differences in mean revertant colony numbers between the application and negative control groups that are significant at the level of $p<0.05$ (Tukey test).

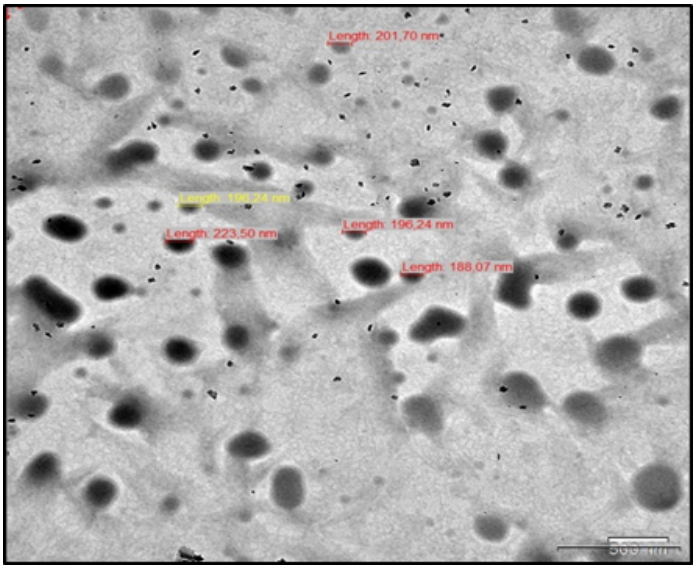

Fig. (6). TEM image of TTO-NPs. (*A higher resolution/colour version of this figure is available in the electronic copy of the article*).

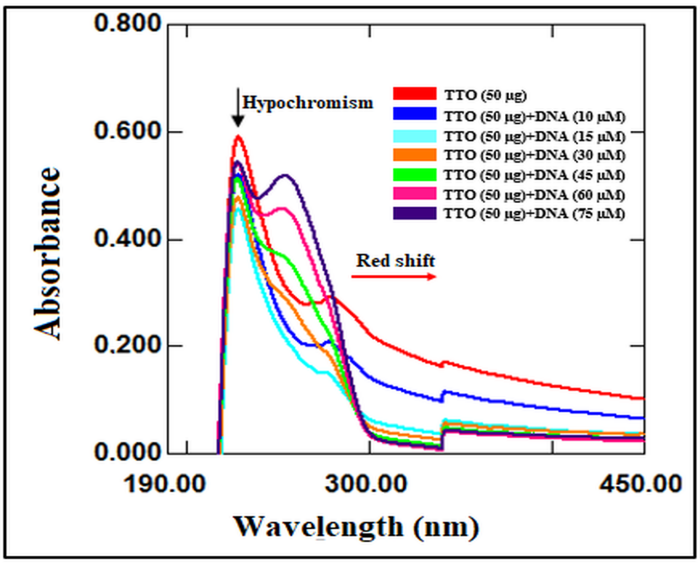

Fig. (7). Absorption spectrum of TTO in the absence (red peak indicated with black arrow) and presence of CT-DNA. (*A higher resolution/colour version of this figure is available in the electronic copy of the article*).

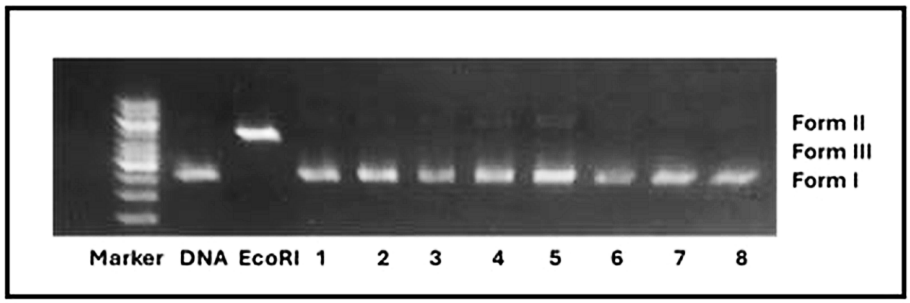

Fig. (8). Electrophoresis image of TTO-NPs and hydrolytic activity of TTO (1: 0.10 mg/mL TTO +DNA, 2: 0.20 mg/ml TTO +DNA, 3: 0.40 mg/mL TTO+DNA, 4: 0.80 mg/mL TTO+DNA, 5: 0.125 mg/mL TTO-NPs+DNA, 6: 0.25 mg/mL TTO-NPs DNA, 7: 0.50 mg/mL TTO-NPs+DNA, 8: 1.00 mg/mL TTO-NPs +DNA). (*A higher resolution/colour version of this figure is available in the electronic copy of the article*).

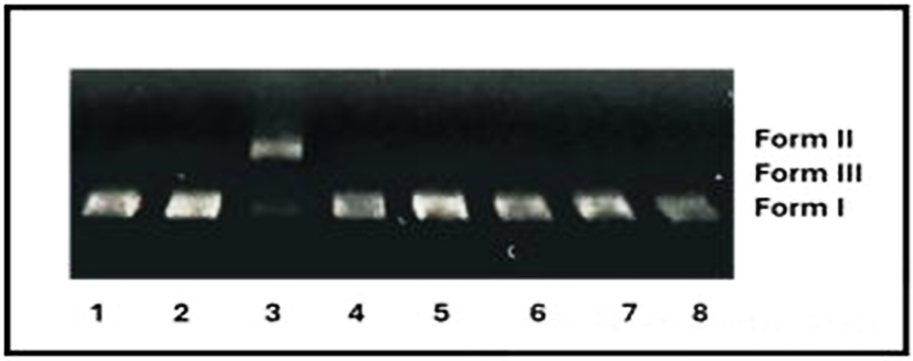

Fig. (9). Electrophoresis image of TTO-NPs and oxidative activity of TTO (1: 0.10 mg/mL TTO+DNA+H_2O_2, 2: 0.20 mg/ml TTO+DNA+ H_2O_2, 3: 0.40 mg/mL TTO+ DNA+ H_2O_2, 4: 0.80 mg/mL TTO+DNA+ H_2O_2, 5: 0.125 mg/mL TTO-NPs+DNA+ H_2O_2, 6: 0.25 mg/mL TTO-NPs +DNA+ H_2O_2, 7: 0.5 mg/mL TTO-NPs +DNA+ H_2O_2, 8: 1.00 mg/mL TTO-NPs +DNA+ H_2O_2). (*A higher resolution/colour version of this figure is available in the electronic copy of the article*).

Table 4. Inhibition zone diameters (mm) of the tested TTO and nanoparticles on bacteria. (N=4).

Bacteria	Particles		
	TTO (Mean±SD)	Blank NPs (Mean±SD)	TTO-NPs (Mean±SD)
Lactobacillus casei	20.59 ± 0.5*	ND	10.01 ± 0.1*
Lactobacillus acidophilus	20.58 ± 0.5*	ND	11.99 ± 0.1*
Streptococcus mutans	11.99 ± 0.1*	ND	20.42 ± 0.5*
Streptococcus wiggsiae	12.13 ± 0.1*	ND	14.04 ± 0.1*

Note: ND: Not determined (no activity observed, 0 mm).
Asterisks (*) indicate that the differences between the zone of inhibition (ZOI) values of the samples and the determined threshold values (>10 mm: effective, ≥20 mm: high sensitivity) are significant at the $p<0.05$ level (T-test).

antibacterial inhibitory activity of TTO, considering the correct binding pose and binding energies. The results of the docking study conducted for terpinen-4-ol and *Streptococcus mutans* glucanosucrase (PDB ID: 3AIC) indicated that the residues of ASP 588 and HIS 587 were the major residues involved in the stabilization of *Streptococcus mutans* Fig. (**10a**, **c**), and the two hydrogen bonds 1.50Å and 2.01Å formed between these residues and terpinen-4-ol supported the stabilization of the complex seen in Figs. (**10b**, **c**).

The active site of DHFR comprises ILE-13, LEU-12, PHE-30, ARG-31, TYR-29, HIS-28, VAL-115 amino acid residues seen in Figs. (**11a**, **b**). The hydrophobic active site pocket of DHFR, which contains the heterocyclic ring system of the substrate or drug, is terminated at one end by the methyl group of THR in α-helix C (THR45 in *Lactobacillus casei*).

In this study, the methyl group of the terpinen-4-ol molecule was directed towards ASP-26 and the distance between them, which does not have a hydrogen bond interaction, was observed as 2.53 Å and 3.82 Å. The methyl carbon of the ALA-6 side chain projects towards the binding site and is in a crucial position for binding the drug with ASP-26. Van der Waals interactions are likely and will stabilize the position of the ligand interacting with the ASP-26 carboxylic acid oxygens in Fig. (**11b**, **c**). Estimates of the two inhibitors' free binding energy were -5.32 kcal/mol for *Streptococcus mutans* and -5.76 kcal/mol for *Lactobacillus casei* dihydrofolate reductase, as seen in Table **5**, respectively.

The binding site interactions and docking score energies of *Streptococcus mutans* with D-Acarbose, 6-Deoxysucrose, Trichloro-galactosucrose, and Myricetin were provided by [50] in Table **5a**.

The interactions at the binding of *Lactobacillus casei* with Trimetrexate [51], Curcumine [52], and a comparison of Methotrexate and Trimethoprim [53] were also given in Table **5b**.

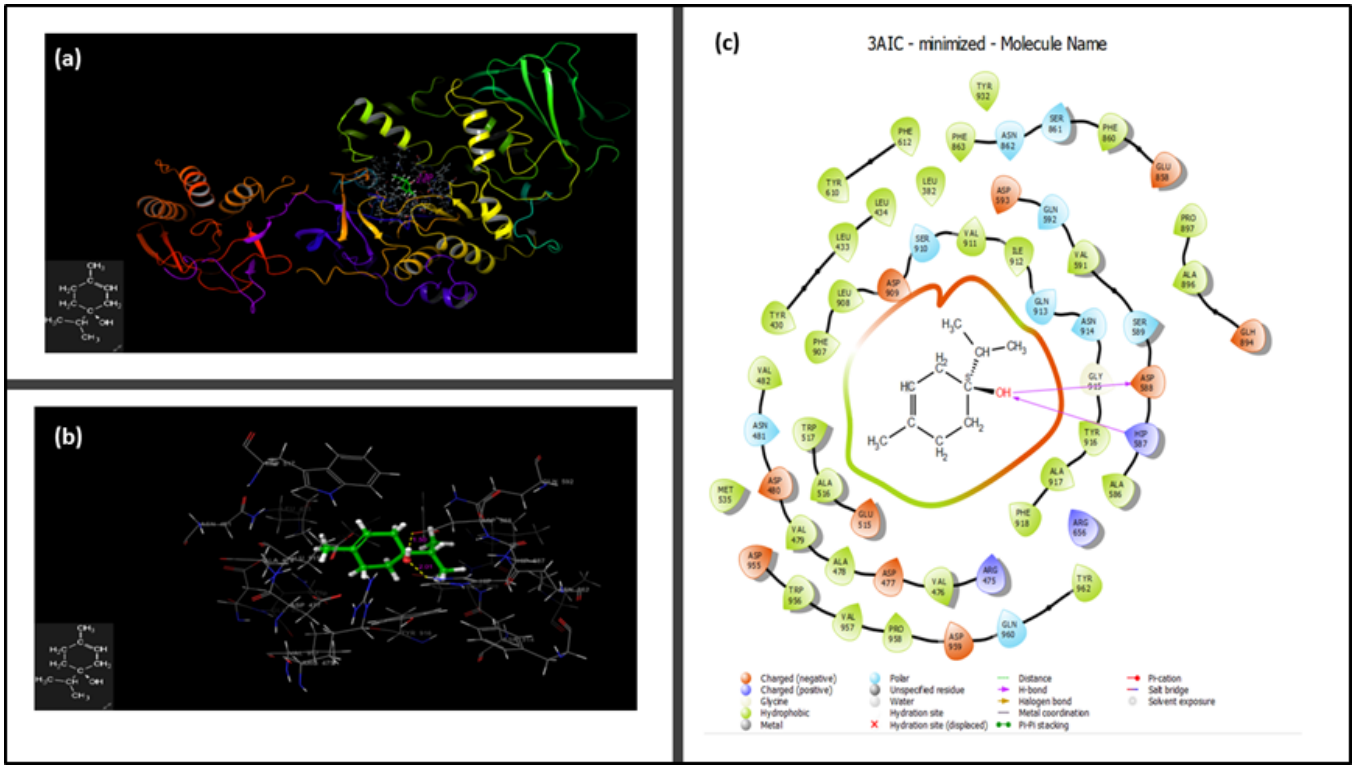

Fig. (10). Represents docking pose of terpinen-4-ol (**a**), hydrogen binding interactions (**b**), binding pocket of *Streptococcus mutans* (PDB-ID: 3AIC) (**c**). (*A higher resolution/colour version of this figure is available in the electronic copy of the article*).

Table 5. The binding site interactions and docking score energies of *Streptococcus mutans*, *Lactobacillus casei* together with terpinen-4-ol.

Table 5a. The binding site interactions and docking score energies of *Streptococcus mutans (PDB ID:3AIC)* and terpinen-4-ol in TTO					
-	**Ligand (Inhibitor) in this Study**	**Ligands (Inhibitor)**			
	Terpinen-4-ol in TTO	***D-Acarbose***	***6-Deoxysucrose***	***Trichloro-galactosucrose***	***Flavonoid Myrecitin***
Docking Score (Kcal/mol)	-5.32	-7.11	-5.31	-5.15	-5.76
H Bonding interaction (Angstrom)	**ASP588 (1.50)** HIS587 (2.01)	GLN960, ASP477, ASP909, HIS587, ARG475, GLU515, **ASP588**	**ASP588,** ASP909, GLN960, ASP477	ARG475, HİS587, **ASP588,** ASP477	TYR916, **ASP588,** ALA478
Table 5b. The binding site interactions and docking score energies of *Lactobacillus casei (PDB ID:1BZF)* and terpinen-4-ol in TTO					
-	***Ligand (Inhibitor) in this Study***	**Ligands (inhibitor)**			
	Terpinen-4-ol in TTO	***Trimetrexate***	***Curcumine PDB:1DRE***	***Methotrexate MTX***	***Trimethoprim TMP***
Docking Score (Kcal/mol)	-5.76	-	-	-	-
H Bonding interaction (Angstrom)	**ILE13 (2.35)** **ALA6 (2.11)**	**LEU4** **ASP26**	**ALA9,** GLU30, PHE31, PHE34, TYR121, VAL115	**ASP26, ALA6,** THR116, LEU4, ALA97, THR45	**ASP26, ALA6,** THR116, LEU4, ALA97, THR45

3.11.2. Molecular Dynamics

The antibacterial activity in TTO is related to its terpinen-4-ol rich chemical composition, terpinen-4-ol-*Streptococcus mutans* and terpinen-4-ol-*Lactobacillus casei* receptor complexes, which indicated the most stable coupling by the docking analysis results, MD simulations were monitored throughout the 50 ns simulation. To form the *Streptococcus mutans*-ligand system, 25308 water molecules and 72 Cl^- and 70 Na^+ atoms were included in the system in Fig. (**12a**), and 6758 water molecules and 23 Na^+ and 19, Cl^- ions were added to the system to form the *Lactobacillus casei*-ligand system seen in Fig. (**12b**).

In Fig. (**13**), *Streptococcus mutans* contact residues (Fig. **13a**), Ligand binding interactions and residue numbers (Fig. **13b**), RMSD (Fig. **13c**), RMSF (Fig. **13d**) and ligand contact (Fig. **13e**) are given.

The RMSD value calculated for *Streptococcus mutans* remained stable for the first 15ns and remained between 1-3 Å and stabilized again at 1.6Å between 40-50 ns, as seen Fig. (**13c**). ASP477 and ASP588 hydrogen binding interactions, TYR-916 with hydrophobic interaction, and ASP-380 with hydrogen bonding effect as seen in Figs. (**13b**, **e**).

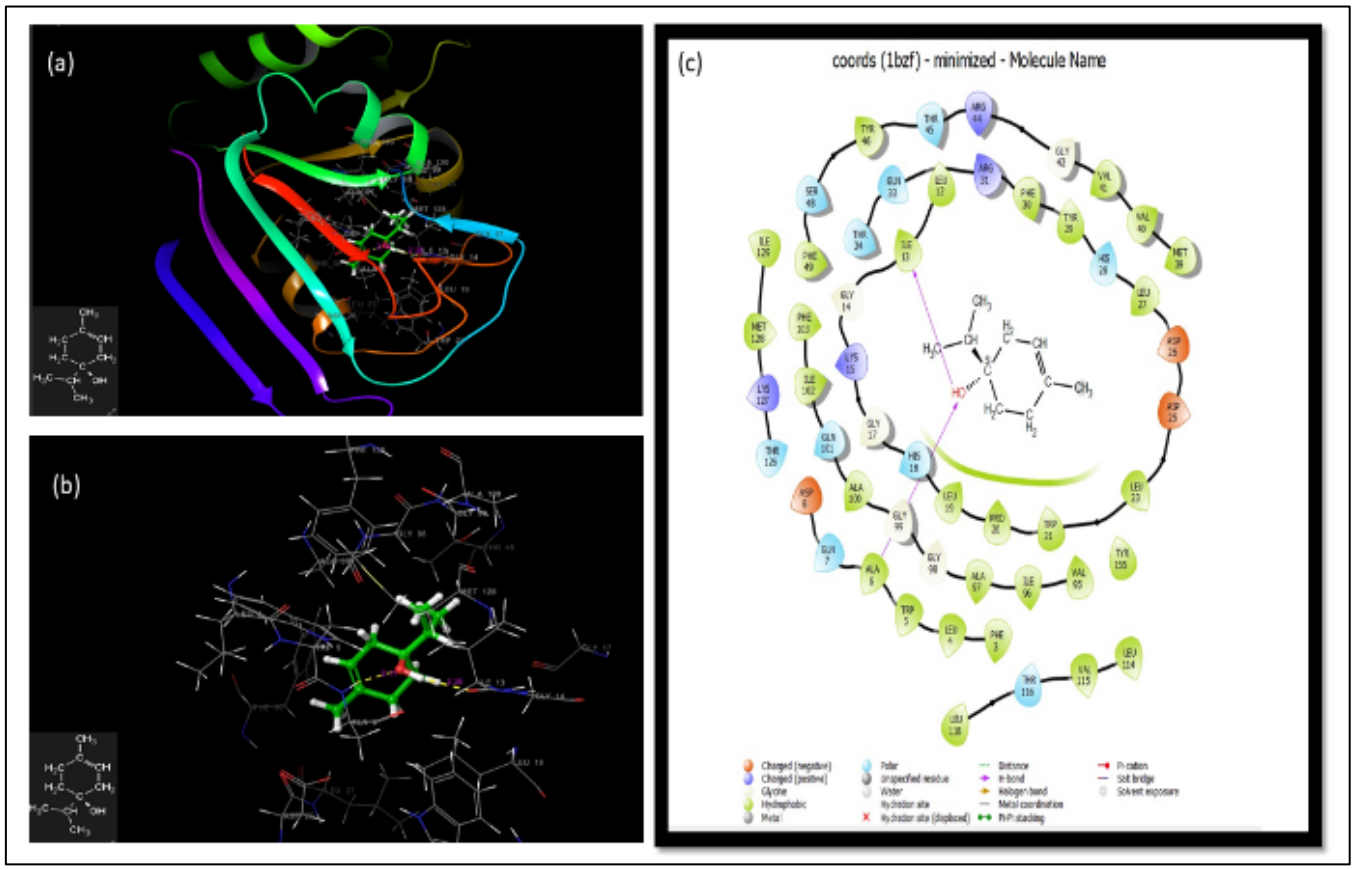

Fig. (11). Represents docking pose of terpinen-4-ol (**a**), hydrogen binding interactions (**b**), binding pocket of *Lactobacillus casei* dihydrofolate reductase (PDB-ID: 1BZF) (**c**). (*A higher resolution/colour version of this figure is available in the electronic copy of the article*).

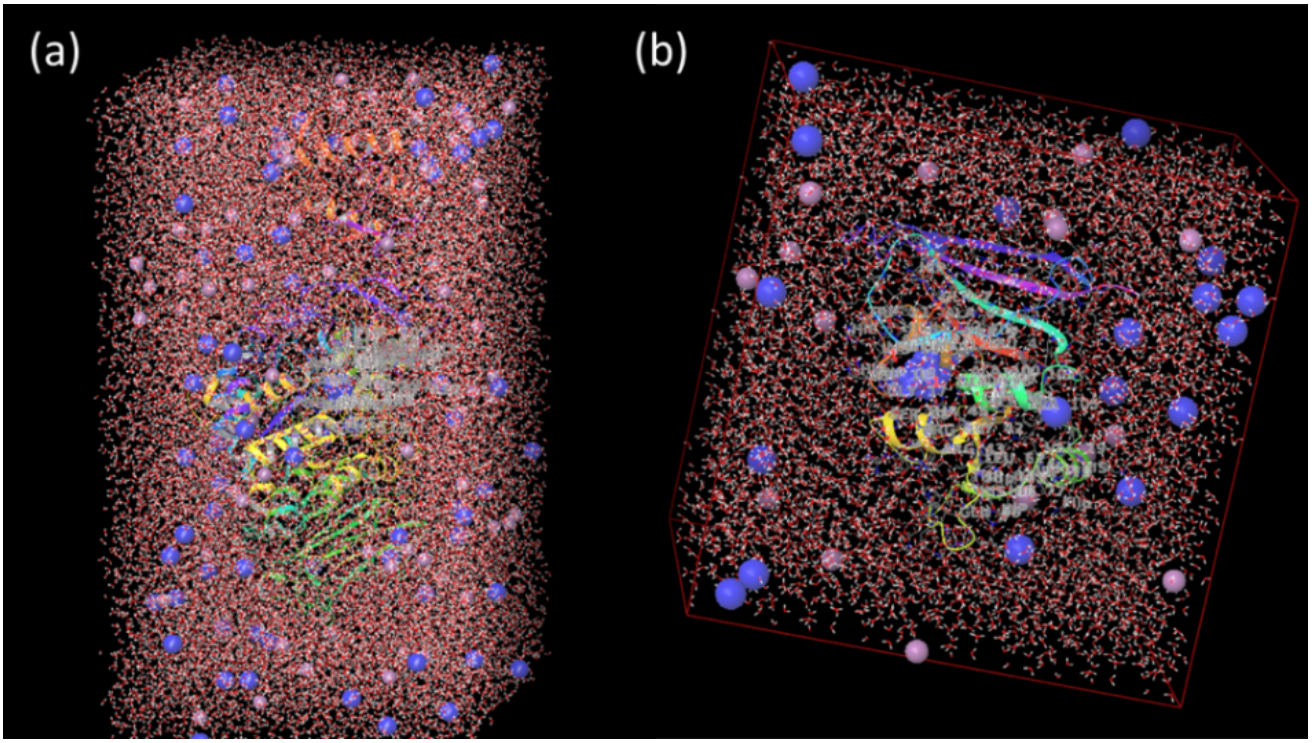

Fig. (12). MD systems for *Streptococcus mutans*-ligand with 25308 water molecules and 72 Cl^- and 70 Na^+ (**a**), *Lactobacillus casei*-ligand system with 6758 water molecules and 23 Na^+ and 19 Cl^- ions (**b**). (*A higher resolution/colour version of this figure is available in the electronic copy of the article*).

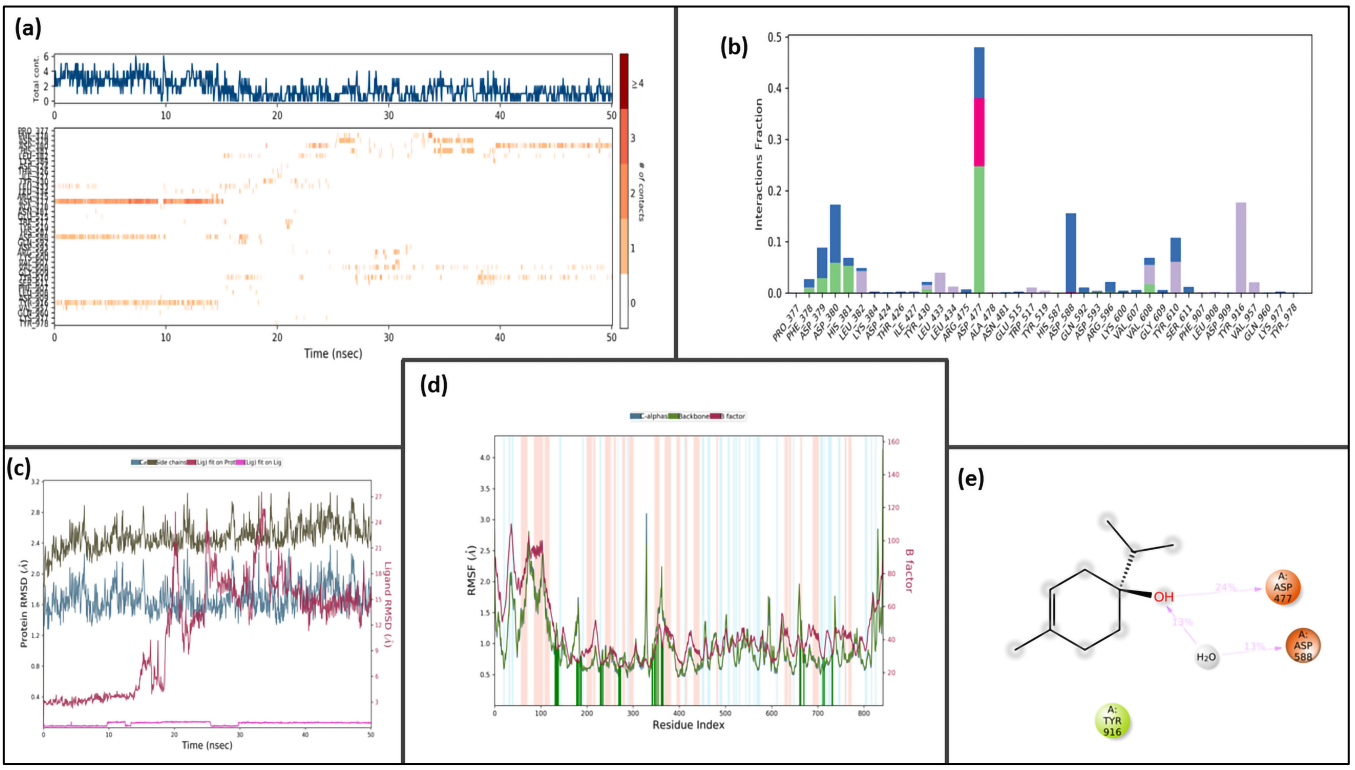

Fig. (13). Contact residues (**a**) and binding interacted residues (**b**), RMSD (**c**), RMSF (**d**) of *Streptococcus mutans* and ligand contact (**e**), in the MD system for 50ns. (*A higher resolution/colour version of this figure is available in the electronic copy of the article*).

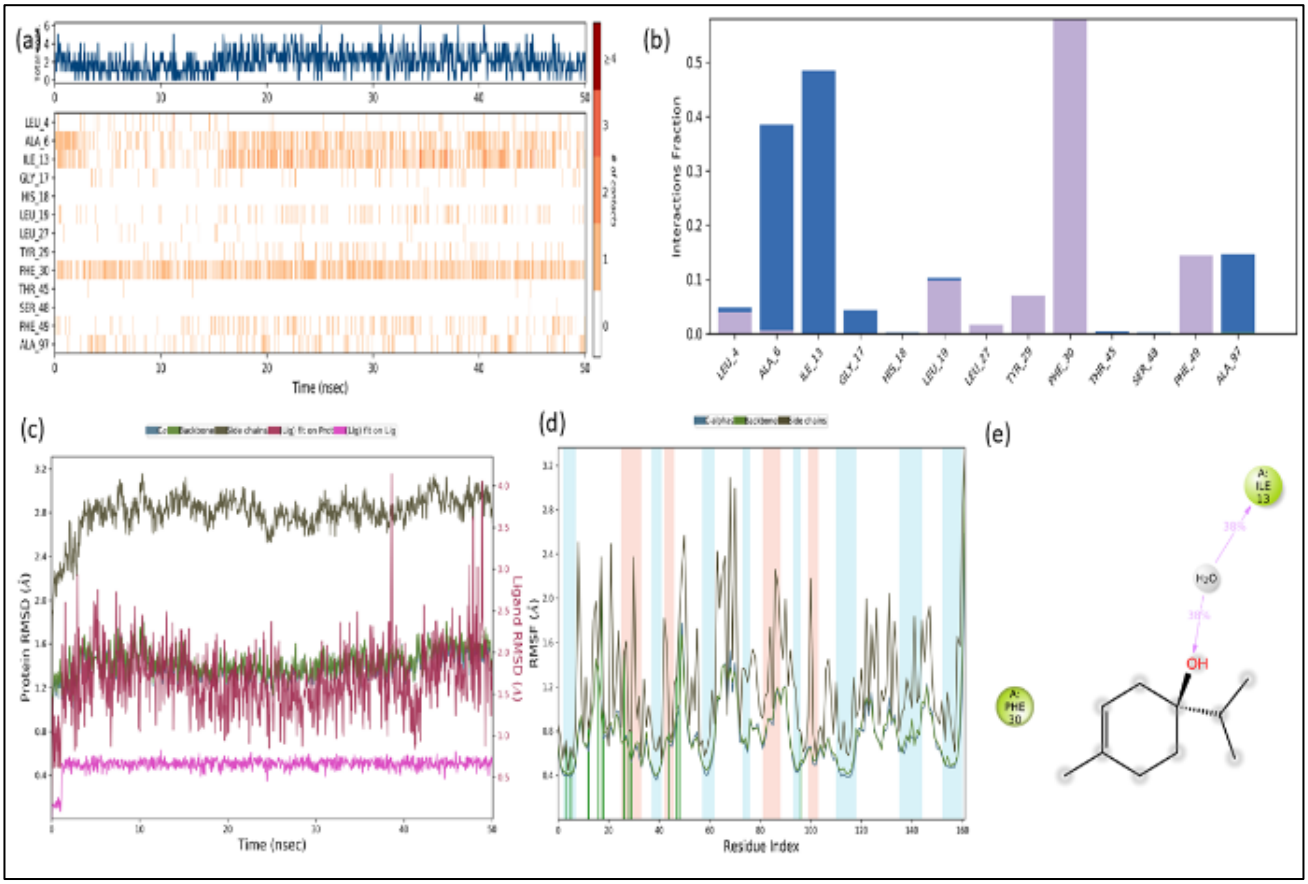

Fig. (14). Contact residues (**a**, **b**), RMSD, RMSF (**c**, **d**) of L. *Lactobacillus casei* and ligand contact (**e**) in the MD system for 50n. (*A higher resolution/ colour version of this figure is available in the electronic copy of the article*).

In Fig. (**14**) *Lactobacillus casei* contact residues (Fig. **14a**), Ligand binding interactions and residue numbers (Fig. **14b**), RMSD (Fig. **14c**), RMSF (Fig. **14d**) and ligand contact (Fig. **14e**) are also given.

It was seen in Fig. (**14c**) that the calculated RMSD value fluctuated around 1.2 Å and 2.8 Å for the first 50 ns and remained stable around 1.2 Å after 20ns. The calculated Ligand RMSD value was also seen as 0.6 Å. From the RMSF graph in Fig. (**14d**), it was seen that there was interaction with the ligand at residues up to 30, between 40-100.

ADME analysis of terpinen-4-ol ligand was calculated by SwissADME platform and is given in Table **6**.

Table 6. ADME properties of Terpinen-4-ol.

Physicochemical Properties	
Formula	$C_{10}H_{18}O$
Molecular weight	154.25 g/mol
Num. heavy atoms	11
Num. arom. heavy atoms	0
Fraction Csp3	0.80
Num. rotatable bonds	1
Num. H-bond acceptors	1
Num. H-bond donors	1
Molar Refractivity	48.80
TPSA	20.23 Å²
Lipophilicity	
Log $P_{o/w}$ (iLOGP)	2.51
Log $P_{o/w}$ (XLOGP3)	3.26
Log $P_{o/w}$ (WLOGP)	2.50
Log $P_{o/w}$ (MLOGP)	2.30
Log $P_{o/w}$ (SILICOS-IT)	2.44
Consensus Log $P_{o/w}$	2.60
Water Solubility	
Log *S* (ESOL)	-2.78
Solubility	2.54e-01 mg/ml ; 1.64e-03 mol/l
Class	Soluble
Log *S* (Ali)	-3.36
Solubility	6.75e-02 mg/ml ; 4.38e-04 mol/l
Class	Soluble
Log *S* (SILICOS-IT)	-1.91
Solubility	1.92e+00 mg/ml ; 1.24e-02 mol/l
Class	Soluble
Pharmacokinetics	
GI absorption	High
BBB permeant	Yes
P-gp substrate	No
CYP1A2 inhibitor	No
CYP2C19 inhibitor	No
CYP2C9 inhibitor	No
CYP2D6 inhibitor	No
CYP3A4 inhibitor	No
Log K_p (skin permeation)	-4.93 cm/s
Druglikeness	
Lipinski	Yes, 0 violation
Ghose	No; 1 violation: M_W<160
Veber	Yes
Egan	Yes
Muegge	No; 2 violations: M_W<200, Heteroatoms<2
Bioavailability Score	0.55
Medicinal Chemistry	
PAINS	0 alert
Brenk	1 alert: isolated_alkene
Leadlikeness	No; 1 violation: MW<250
Synthetic accessibility	3.28

4. DISCUSSION

The antibacterial effectiveness of TTO has been proven with its polyphenol content, which was found to be 45.476 % terpinen-4-ol as the major compound, 22.039% γ-terpinene, and 9.748 % α-terpinene, respectively. These findings are in accordance with the literature in terms of providing an effective mouth hygiene [21, 24].

The size of nanoparticles plays a crucial role in their antibacterial activity, as well as in their interaction with bacteria and biofilms [54-56]. The average particle size of TTO-NPs was 221.6 nm, the PdI value was 0.103, and the zeta potential value was -5.22 mV According to our results, the average particle size values of TTO-NPs and blank NPs were 221.6 nm and 196.4 nm, respectively. These results were compared with other studies in the literature for dental applications. The average particle size of PLGA nanoparticles loaded with 10 and 25 mg of clove oil was 165.37 ± 22.53 and 237.63 ± 13.68 nm, respectively [57]. The hydrodynamic diameter of amphiphilic quaternized chitosan nanoparticles, which possess anti-cariogenic biofilm properties, was approximately 100-300 nm [58]. In the study of Ferreira *et al.* [59], the average size of TTO-loaded PCL nanoparticles was determined to be in the 180-220 nm range. The mean particle size of curcumin-loaded PLGA nanoparticles developed against endodontic biofilms was 247.6 ± 3.651 nm [60]. Moreover, it was demonstrated that the mean particle sizes of PLGA nanoparticles loaded with cinnamon bark and orange peel essential oils, synthesized to prevent dental caries, were 219 ± 4.49 nm and 243.1 ± 0.60 nm, respectively. The combination of two essential oils was effective against L. casei and *S. mutans* bacteria [61]. Therefore, it was concluded that TTO-NPs have a suitable size range for dental applications. In our study, the DLS analysis showed that the TTO-NPs were obtained with an average particle size of 221.6 nm, and the blank NPs had an average particle size of 196.4 nm.

On the other hand, TTO-NPs had a higher average particle size compared to blank NPs. Other studies in the literature similarly supported the increase in average particle size after the addition of an active ingredient. This is most likely due to the volume occupied by the essential oil as a result of encapsulation, resulting in an increase in average particle size [62]. It is desirable for nanoparticles to exhibit a monodisperse size distribution to be effective, safe, stable, and have predictable properties [63]. Moreover, monodisperse nanoparticles are preferred to obtain improved therapeutic results [64]. In this context, the PdI value relatively shows the particle size distribution of colloidal systems. In general, PdI values less than 0.2 are considered monodisperse, while those greater than 0.2 are considered polydisperse [65]. Our DLS results showed that blank NPs and TTO-NPs had PdI values of 0.124 and 0.103, respectively.

Panyam *et al*. showed that a polydispersity index (PdI) up to 0.2 is considered a monodisperse formulation for PLGA NPs [66]. Moreover, in many studies on essential oil-loaded PLGA nanoparticles in the literature, it has been reported that the PdI value is 0.2 or less, and the colloidal system is monodispersing [67-69]. In another study, it was reported that *Ferula assa-foetida* loaded PLGA nanoparticles were synthesized. It was stated that these therapeutic nanoparticles had good antibacterial effects with the 203.62 nm average particle size and the 0.264 PdI value [70]. In this context, it was understood that the TTO-NPs synthesized within the scope of our study exhibited monodisperse size distribution as desired for high therapeutic success. Zeta potential is a measure of the electrical potential at the interface between particles and a surrounding liquid medium. Zeta potential value can provide important information about nanoparticles' stability and their possible interactions with biological systems [71]. Our DLS results showed that blank NPs and TTO-NPs had zeta potentials of -6.08 mV and -5.22 mV, respectively. These results were compared with other studies in the literature. Gursu *et al*. [72] reported that cinnamaldehyde-loaded PLGA nanoparticles exhibited good stability with zeta potential values ranging from -3.54 to -3.86 mV. Minhaco *et al.* [60] synthesized curcumin-loaded PLGA nanoparticles to treat endodontic biofilms with zeta potential values of -1.65 ± 0.355 mV. In this context, it was concluded that the TTO-NPs have a higher zeta potential value compared to those reported in the literature.

The encapsulation efficiency and the loading capacity of TTO-NPs were determined *via* Equations 1 and 2 as 88.57% and 62%, respectively. In a study completed in 2016, it was observed that the encapsulation efficiency was around 96.08% [47]. The encapsulation efficiency of 88.57% calculated in our study was found to be close to the data given in the literature. It was observed that the difference might be due to the volatility of the essential oil. Khan *et al.* [73] obtained PLGA nanoparticles loaded with doxorubicin and berberine and investigated the effect of these nanoparticles in cancer treatment. The trapping efficiency and drug loading of the obtained nanoparticles were found to be 52.98 ± 1.58% and 12.8 ± 1.35% (%w/w), respectively. Loading efficiency affects release time, as the release profile requires sustained release over a longer period of time. The low loading capacity resulted in a reduced release time [73]. Consequently, the loading efficiency was calculated as 62% in our study, and it was observed that this had a positive effect on the release time.

The release profile of the TTO-NPs was assessed as a function of time. It was determined that the *in vitro* release study results showed a biphasic release pattern (Fig. **4**). A faster release in the first 5 hours was followed by a slower release from the 6th hour to 72 hours. This kind of release profile occurs because the essential oil molecules adsorbed on or near the nanoparticle surface have been located [68, 74]. After the 6th hour, the slower release phase occurred with the diffusion of encapsulated essential oil molecules from the polymer matrix into the release medium. When the *in vitro* release of free TTO was evaluated under the same conditions, it was observed to be rapidly released at a rate of 99.98% ± 1.24% in the sixth hour. Ercin *et al.* [32] reported that essential oil-loaded PLGA nanoparticles exhibited 72 hours *in vitro* release profile. In our study, TTO was almost entirely released from TTO NPs within 72 hours. This result was similar to that found in essential oil-loaded polymeric nanoparticle formulations in the literature [68, 74]. It was reported that the *in vitro* release profile of the essential oil from the nanoparticles can be based on the formulation parameters, such as the molecular weight and electrical charge of the polymer, essential oil concentration, and average particle size [74-76].

ATR-FTIR spectra ATR spectra for blank NPs, TTO-NPs, and TTO were captured in three distinct areas (Fig. **5**). It is thought that the broad band observed in the spectrum between 3400 cm^{-1} and 3300 cm^{-1} is mainly due to the OH contribution of molecules such as terpinen-4-ol and α-terpineol in TTO. The peaks of TTO at 2960 cm^{-1}, 2915 cm^{-1}, 2877 cm^{-1} were observed in TTO-NPs at 2938 cm^{-1} and 2915 cm^{-1}. This region corresponds to the C-Hs found in the TTO to the stretching vibrations caused by the presence of -C-H bonds in almost all the components in the TTO. The peak at 1641 cm^{-1} for TTO and TTO-NP spectra was attributed to C=C stretching. The C-H bending vibrations in compounds like terpinen-4-ol contributed to the formation of sharp peaks at 1444 cm^{-1} in the TTO spectrum. Also, it is thought that the alkaloid C-O bonds in these compounds contributed to a sharp peak at 1068 cm^{-1}. The C-O bond present in the TTO spectrum contributes to the sharp peak of high intensity at 1026 cm^{-1}. The region between 948 cm^{-1} and 721 cm^{-1} corresponds to =C-H bending vibrations of the compounds in the TTO. The peak observed at 924 cm^{-1} in TTO was not observed in TTO-NPs. The presence of TTO-related peaks in the spectrum of TTO-NPs showed that TTO was present in the structure of TTO-NPs, and the all peaks observed for TTO correspond [48]. In literature, the pure terpinen-4-ol presents absorption bands at 889 cm^{-1}, 864 cm^{-1}, and 799 cm^{-1} in the TTO spectrum. Similar peaks at 886 cm^{-1}, 864 cm^{-1}, and 798 cm^{-1} were also observed for terpinen-4-ol in the TTO spectrum [77]. Ocak *et al*. [78] performed FT-IR spectroscopy analysis of gelatin-coated TTO nanoparticles. The determined TTO strong absorption peak was found at a wavelength of 1737 cm^{-1}, and when the absorption peak of TTO loaded gelatin nanoparticles was examined, it was seen that it remained unchanged at a wavelength of 1737 cm^{-1}. In this study, this peak was seen at 1737 cm^{-1} for only TTO-NPs. Figure 5 illustrates the spectra of TTO, TTO-NPs, and blank NP, allowing for an in-depth exploration of their unique peaks. In (a), the expansive 4000-2400 cm^{-1} region, (b) the 1800-1000 cm^{-1} region, and (c) the 1100-500 cm^{-1} region.

Unlike DLS analysis, TEM analysis is an imaging method that provides a better understanding of the actual geometric size of nanoparticles and information about their morphology [49]. In our study, the morphology analysis of TTO-NPs was performed by using TEM. As seen in Fig. (**6**), the nanoparticles were dispersed, and the TTO-NPs were spherical in shapes and had smooth surfaces. However, a slight aggregation tendency was observed in some of the particles. In a study conducted in 2021, it was seen by TEM analysis that piperine-loaded PLGA nanoparticles had a smooth outer surface and a spherical shape. It was reported that the low surface roughness was found to be effective in controlled drug release [79]. In our study, TTO-NPs were also found to be uniformly distributed and spherical. From the images obtained through TEM analysis, it was determined that the diameter of the particles ranged from 188.07 nm to 223.50 nm. Additionally, the dynamic light scattering results of TTO-NPs revealed an average particle size of 221.60 nm. Although the obtained results are quite close to each other, it is thought that there are slight size differences due to methodological differences because DLS analysis measures the average particle size of the colloidal system, whereas TEM analysis is based on the real-time analysis of particle sizes *in situ*.

One of the first targets of antibacterial drugs is DNA, and UV-Vis spectroscopy is one of the fundamental techniques for studying small molecule-DNA interactions, which investigates the variations in absorbance magnitude (hyper- or hypochromism) and peak position (blue- or red-shift), which are related to the strength of the interaction [35]. In general, tiny molecule non-covalent interactions with DNA are connected to hyperchromism, whereas an intercalative mode may lead to hypochromism and red shift [33]. The interaction of TTO with DNA showed (Fig. **7**) that when CT-DNA was added successively, 46.5% hypochromism at 236.40 nm (indicated by the black arrow) and a red shift of 9 nm (indicated by the red arrow) were observed in the UV-Vis absorption of TTO. The UV-Vis absorption spectrum precludes analyzing small and conformational groups of biomacromolecules

[80]. In the DNA binding assay, absorbance amplitude (hyperchromism) and shift of peaks (blue determination) are detected [81]. Intercalative is related to hypochromism and redshift. In a study, it was stated that 14 nm hypochromic shifts of essential oil were observed at a high rate [82]. In the literature review, it was seen that DNA binding analysis of TTO was not performed. The 9 nm hypochromic shift observed in our study matched the result of intercalative binding of essential oils to DNA seen in studies.

The ability of TTO-NPs and TTO to fragment DNA was evaluated using the agarose gel electrophoresis method (Figs. **8** and **9**). TTO-NPs did not react with DNA, resulted in no activity being seen. Encapsulation of TTO with the PLGA polymer prevented TTO from interacting directly with the DNA, thereby preventing oxidative damage to the DNA and acting as a barrier. The mutagenic activity of essential oils has been the subject of many studies in the literature [83-86]. Various studies have reported that the encapsulation of essential oils with polymer contributes to the prevention of mutagenic activity [86, 87]. It has been recognized as a strategic approach to formulating them as a controlled release system to eliminate the problem of the genotoxicity of EOs. In our study, the mutagenicity of TTO and TTO-NPs was evaluated with the Ames test. In experiments using TA98 and TA100 strains, results were evaluated using positive, negative, and spontaneous controls (Tables **2** and **3**), respectively. The results showed that the applied concentrations of TTO-NPs were not mutagenic. However, concentrations of TTO (0.10, 0.20, 0.40, and 0.80 mg/mL) were found to cause both frameshift mutation (TA98) and base change mutation (TA100). In addition, it was observed that the number of returned colonies on the plate of TTO (0.40 and 0.80 mg/mL) was very low. It was reported in various studies that the number of colonies returned on the plate is quite small. This is because the sample used is toxic [86-88]. It was evaluated that all concentrations of TTO were mutagenic ($p < 0.05$). Shoeibi *et al.* [89] in their study examining the mutagenic effects of four different essential oils, reported that the concentrations in the range of 50 and 2000 µg/mL of *Cinnamum zeylanicum, Thymus vulgaris,* and *Zataria multiflora* essential oils had no mutagenic effect. However, they reported that clove essential oil was mutagenic at 500 µg/mL and higher concentrations. In a study, the mutagenic potential of TTO was examined with the aid of the Ames assay by Casalle *et al*. [90], and they reported that none of the TTO concentrations increased in colony count over the negative (solvent) control values obtained from strains TA100 and TA98. The result demonstrated that the concentrations of TTO did not generate any base pair or frameshift mutations. However, in our study, a mutagenic feature was observed for all concentrations of TTO ($p < 0.05$). In contrast, mutagenicity was not observed for the TTO-NPs. The results showed that TTO NPs were not mutagenic ($p < 0.05$) in TA98 and TA100 strains due to their controlled release properties, consistent with literature studies [91, 92].

Our results are consistent with studies reporting that EOs are not genotoxic when formulated as a controlled-release system encapsulated with a polymer. Nearly all doses of TTO were found as mutagenic, while not all doses of TTO-NPs were mutagenic. Formulation in nanoparticle dosage forms eliminated the mutagenicity of TTO. The results of our study indicate that the mutagenicity of TTO-NPs is formulation-dependent, and the encapsulation strategy helped decrease the mutagenicity of the essential oil.

Agar diffusion assays are commonly employed to evaluate the antimicrobial activity of natural products. A zone of inhibition (ZOI) of 10 mm or more typically indicates antimicrobial activity, while ≥15 mm is considered high sensitivity [93]. For all bacterial species, the inhibition zone diameter of the blank NPs group was measured as 0 mm, confirming that the antimicrobial effects were due to TTO and TTO-NPs. On the other hand, it was determined that bacteria were very sensitive to TTO; similarly, TTO-NPs were found to be effective on these bacteria (Table **4**). TTO was more effective against *Lactobacillus species*, while TTO-NPs showed superior activity against *Streptococcus* species, especially *S. mutans. Lactobacillus casei* and *Lactobacillus acidophilus* are gram-positive, rod-shaped bacteria that do not form spores or flagella. In contrast, *Streptococcus mutans* and *Streptococcus wiggsiae* are gram-positive, non-spore-forming cocci [94, 95]. Our results supported the notion that TTO-NPs with controlled release and a negatively charged surface could selectively inhibit streptococci more effectively while inhibiting lactobacilli to a lesser extent. Additionally, it was found that TTO interacted more effectively than TTO-NPs with *Lactobacillus* species. TTO-NPs, which we determined to have a spherical morphology by TEM analysis, exhibited different interactions with bacteria of varying morphologies, such as rods and cocci, due to their negative surface charge. The obtained results indicated that TTO-NPs interacted more effectively with *Streptococcus mutans* and *Streptococcus wiggsiae*, which are non-spore-forming cocci, and exhibited higher inhibition compared to the Lactobacillus species.

The most important parameters affecting the interaction of nanoparticles with bacteria are their surface chemistry, increased surface area at the nanoscale, and morphology [96]. For example, the large surface area of spherical nanoparticles allows them to interact more effectively with bacteria and penetrate the bacterial cell membrane. This, in turn, allows for the disruption of bacterial molecular mechanisms [54]. The large surface area of TTO-loaded PLGA nanoparticles creates more interaction sites with the bacterial cell wall, which consists of the peptidoglycan layer, and by forming various interactions, including primarily hydrophobic interactions, hydrogen bonds, and van der Waals interactions, they contribute to biofilm inhibition and the penetration of the active ingredient, TTO, into bacteria [96, 97].

Dental caries demineralizes the tooth structure day by day. It is caused by cariogenic bacteria, especially *Streptococcus mutans*, which adhere to the tooth and play a role in developing dental caries [98]. As a result, medications specifically targeting the cariogenic bacterium are thought to be the best way to treat dental caries [99]. The caries inhibition activity of the TTO-NPs developed in this study was matched with the data described in the literature.

TTO is an essential oil made from the leaves of the *Melaleuca alternifolia* plant through distillation [100]. Essential oil constituents interact with bacterial structural components. The antibacterial activity of this interaction is crucial. Terpinen-4-ol, which is determined as the major component among the active components in the TTO structure, is thought to be responsible for the antibacterial effect of TTO [101]. It was reported by *in vitro* studies that TTO showed antimicrobial activity [100]. In a study examining the effectiveness of TTO and TTO-loaded metallic nanoparticles on different dental caries-causing bacteria, the authors reported that free TTO was more effective than TTO-loaded metallic nanoparticles. This situation can be explained by the fact that TTO-loaded metal nanoparticles cannot trap enough TTO during synthesis; metal NPs tend to collapse and cluster, thus reducing biological interaction interfaces due to the decrease in surface area ratio and the functional groups that will show bioactivity of the phytochemical (TTO) bound to the metal NP core remain in the inner part (inactive region). In our study, it was determined that TTO-NPs were effective on four different bacteria, especially on *Streptococcus mutants* [25]. Kanth *et al.* [102] stated that it could be inferred that natural products have the maximum effectiveness against microorganisms and can be recommended in dentifrices, mouth rinses, topical gels, *etc*. TTO was shown to affect *Staphylococcus* and *Streptococcus* species [59] significantly. In addition, the antifungal [103], anti-inflammatory [104, 105], and antiviral [105] effects of TTO have been proven. Li *et al.* [30] studied the effectiveness of TTO on *Escherichia coli* and

Streptococcus mutans bacteria. They reported that no colony was observed in either bacterium. In this study, it was found that TTO-NPs had antimicrobial activity on *Lactobacillus casei*, *Lactobacillus acidophilus*, *Streptococcus mutans,* and *Scardovia wiggsiae.* The biodegradability, biocompatibility, and biosafety of the PLGA, found as a coating material in TTO-NPs, are known [106]. Our results showed that blank PLGA nanoparticles applied to bacteria did not cause any effects on the bacteria. Mechanical clearance is still of the utmost relevance among all dental biofilm-controlling strategies. However, instead of eliminating the oral microflora, chemical therapy offers a substitute or supplemental approach by reducing the buildup of biofilm [107]. Topically applied antibacterial drugs can not demonstrate effectiveness at acceptable concentrations for a long enough period due to the complexity of the oral microbiota and the inability of saliva to remain in the mouth for the needed time [108]. According to Yallapu *et al.* [106], new nanomaterials that carry antimicrobial drugs/molecules or function as pharmaceuticals can precisely target the pathogen in response to particular environmental cues. Additionally, potential therapeutics to disrupt oral biofilm are specially created small compounds that target important mediators of bacterial adhesion.

Molecular docking analysis was performed using *Streptococcus mutans* (PDB ID: 3AIC) and *Lactobacillus casei* dihydrofolate reductase (PDB ID: 1BZF) receptors to predict the antibacterial inhibitory activity of TTO, considering the correct binding pose and binding energies. *Streptococcus mutans* is a gram-positive, acidic, and acidogenic bacterium that causes caries development by allowing colonization of the tooth surface, including its high biofilm-forming capacity. Glucansucrases or glycosyltransferases (GTFs) are extracellular enzymes produced by various bacteria, including *Streptococcus mutans*, that break down sucroseinto glucose and fructose and form adhesive biofilm chains. Glucan chain growth is also associated with the adhesion of one bacterium to another and to the tooth surface. Preventing the formation of this microbial complex is one of the most targeted strategies for caries control [109]. Glucanosucrase in *Streptococcus mutans* also allows the metabolism of sucrose to lactic acid, which lowers the pH around the teeth and facilitates the dissolution of calcium phosphate from tooth enamel, which causes tooth decay. These properties make *Streptococcus mutans* glucanosucrase one of the primary and most studied targets in the development of new agents useful in the prevention of dental caries. The amino acid residues ASP-588, TRP-517, and ASN-481 of the A1 domain of the enzyme proved to be vital for the inhibitory effect and binding of all carbohydrate derivatives (6-Deoxy sucrose and Trichloro galactosucrose) to these residues. This enabled them to be identified as the most promising GtfC inhibitors [50]. The results of the docking study conducted for terpinen-4-ol and *Streptococcus mutans* glucanosucrase (PDB ID: 3AIC) indicated that the residues of ASP 588 and HIS 587 were the major residues involved in the stabilization of *Streptococcus mutans*, and the two hydrogen bonds 1.50 Å and 2.01 Å formed between these residues and terpinen-4-ol supported the stabilization of the complex (Fig. **10b**, **c**).

The active binding site encompasses GLU515, ASP588, ASP477, ARG475, HIS587, TYR916, TYR430, LEU433, ASN481, and TRP517. Looking at the binding efficiency and interactions of reference ligand D-Acarbose into the *Streptococcus mutans*, amino acid residues in subsite-1 (ARG475, ASP477, GLU515, HIS587, and ASP588) established hydrogen bonds with oxygen and nitrogen atoms of D-Acarbose. The inhibitory activity of D-Acarbose can be explained by its stable interaction, especially with GLU515, ASP477, ASP588, LEU433, TRP517, and ASN481 residues [50]. For deoxysucrose, which has a high inhibitory effect, this effect can be attributed to the multiple hydrogen bonds with ASP588. Multiple hydrogen bonding with the Subsite −1 amino acids, including GLU515, ASP477, ARG475, HIS587, and ASP588, stabilizes the inhibition complex of *Streptococcus mutans*. In this study, terpinen-4-ol, a major compound in TTO, was specifically attributed to its stable interaction with strong hydrogen bonding between ASP588 and HIS587 in Fig. (**10b**, **c**). Dihydrofolate reductase (DHFR) plays a critical role in regulating folate metabolism, and therefore, DHFR is essential for purine and thymidylate synthesis and cell growth and proliferation. Because of that, DHFR has been a primary focus in developing anticancer and antibacterial reagents. DHFR is of pharmaceutical importance as another drug target against bacterial, fungal, and protozoan infections [110, 111]. Antifolate drugs are widely used in medicines for the treatment of tumor diseases (Methotrexate, MTX), (Trimethrexate TMQ), bacterial infections (Trimethoprim TMP), and protozoan infections (Pyrimethamine, PMX) by blocking the DHFR enzyme functioning [112]. The active site of DHFR comprises ILE-13, LEU-12, PHE-30, ARG-31, TYR-29, HIS-28, VAL-115 amino acid residues as seen in Figs. (**11a**, **b**). Two hydrogen-bonding interactions (2.35Å and 2.11 Å) were observed between active site residues ILE-13 and ALA-6 with the OH group of terpinen-4-ol in Figs. (**11b**, **c**). The active site of DHFR was given by [52] the ILE-7, LEU-22, PHE-31, PHE-34, ARG-70, VAL-115, and TYR121 residues. The ligand curcumin also appears to bind in the active site by making extensive van der Waals contacts. The nonpolar interactions occur with the side chains of ILE-7, ALA-9, and VAL-115 with some main chain atoms of VAL-8 and ALA-9 for MTX binding, and similar nonpolar interactions were observed for curcumin at residues ILE-7, ALA-9, LEU-22, and VAL-115 [52]. In this study, the hydrophobic ALA-6 residue interacted with hydrogen bonding with the terpinen-4-ol's hydroxy group. The hydrophobic active site pocket of DHFR, which contains the heterocyclic ring system of the substrate or drug, is terminated at one end by the methyl group of THR in α-helix C (THR45 in *Lactobacillus casei*). DHFR revealed several significant interactions of the THR-45 residue within the active site [53]. Methotrexate (MTX) has the -CH2-carbon 4.3 Å from the methyl carbon of THR45 in the ternary complex. The distances from drug molecules like Methotrexate, Trimethoprim, Pyrimethamine, Cycloguanil, and Chlorcycloguanil have been given 4.3 Å, 5.4 Å, 2.1 Å, 1.8 Å, and 1.9 Å, respectively [53]. In this study, the distance from the terpinen-4-ol is given by 4.44 Å. It is not recommended that the van der Waals distance for the contact and interaction between terpinen-4-ol and the methyl carbon of the THR45 side chain be less than 3.6 Å, and our ligand placement pose is suitable for this distance.

The substructure-domain interactions validated from [51] give the distance between Trimetrexate against the dihydrofolate reductase domain with LEU-4 residue as 3.2 Å by hydrogen bonding interaction. In this study, the distance from the LEU-4 residue was calculated by 3.45 Å. The two hydrogen bonding interactions (3.16 Å and 3.18 Å) occurred between the O atoms of ASP-26 and the N atoms of Trimetrexate. In this study, the methyl group of the terpinen-4-ol molecule was directed towards ASP-26, and the distance between them, which does not have a hydrogen bond interaction, was observed as 2.53 Å and 3.82 Å. The methyl carbon of the ALA-6 side chain projects towards the binding site and is in a crucial position for binding the drug with ASP-26. Van der Waals interactions are likely and will stabilize the position of the ligand interacting with the ASP-26 carboxylic acid oxygens. Estimates of the two inhibitors' free binding energy were -5.32 kcal/mol for *Streptococcus mutans* and -5.76 kcal/mol for *Lactobacillus casei* dihydrofolate reductase, as seen in Table **5**, respectively.

The antibacterial activity in TTO is related to its terpinen-4-ol rich chemical composition, terpinen-4-ol-*Streptococcus mutans* and terpinen-4-ol-*Lactobacillus casei* receptor complexes, which indicated the most stable coupling by the docking analysis results. MD simulations were monitored throughout the 50 ns simulation.

To form the *Streptococcus mutans*-ligand system, 25308 water molecules and 72 Cl^- and 70 Na^+ atoms were included in the system in Fig. (**12a**), and 6758 water molecules and 23 Na^+ and 19 Cl^- ions were added to the system to form the *Lactobacillus casei-ligand* system seen in Fig. (**12b**). Calculated root mean square deviation (RMSD) and root-mean-square fluctuations (RMSF) analyses were provided by MD trajectories for analysis of the stability of ligand-receptor complexes. Receptor-Ligand interactions were also defined by contact times and contact sites.

The RMSD value of the receptors, which allows us to analyze the simulation balance, can give an idea of the structural conformation of the receptors throughout the entire process. Changes at the 1-3 Å are acceptable, indicating that the receptors did not undergo a major conformational change during the simulation. The RMSD value calculated for *Streptococcus mutans* remained stable for the first 15 ns and fluctuated between 15 ns and 40 ns (Fig. **13c**). This value remained between 1-3 Å and stabilized again at 1.6 Å between 40-50 ns, as seen in Fig. (**13**). During this whole process, the ligand RMSD value remained below 0.4 Å and preserved its stable structure. The peaks in the calculated RMSF plot in Fig. (**13d**) indicated the parts of the receptor that fluctuated the most during the simulation. The overlap in the calculated RMSF and B factor plots indicates that the simulation results align with the crystallographic data of *Streptococcus mutans*. Residue contacts interacting between *Streptococcus mutans* and the ligand were also shown with green lines. Among the interactions between Streptococcus mutans and ligand, PHE-378, ASP-379, ASP-380, HIS-381, TYR-430, ASP-477, and VAL-608 provided interaction with hydrogen bonding in Fig. (**13b**). Both hydrogen bonding and ionic interaction took place between ASP-477 and the ligand (see in Fig. **13b**). The ASP-588 interaction due to docking was observed here as an ionic interaction with the water effect. During the simulation, the most interacting residues were ASP-477 in Fig. (**13a**) with hydrogen bonding and ionic interactions with 24%, ASP-588 with ionic interaction with 13%, TYR-916 with hydrophobic interaction, and ASP-380 with hydrogen bonding effect as seen in Figs. (**13b**, **e**).

Similar residues in subsite-1 (ARG475, ASP477, GLU515, HIS587, ASP588) in the binding interactions of D-Acarbose to *Streptococcus mutans* enabled D-Acarbose to show inhibitory activity. These residues interacted with D-Acarbose, 6-Deoxysucrose, Trichloro-galactosucrose, and also Flavonoid Myrecitin [50].

In our study, the calculated RMSD value fluctuated around 1.2 Å and 2.8 Å for the first 50 ns and remained stable around 1.2 Å after 20 ns (Fig. **14c**). The calculated Ligand RMSD value was also seen as 0.6 Å. From the RMSF graph, it was seen that there was interaction with the ligand at residues up to 30, between 40-100 in Fig. (**14d**). The most interacting ones during 50 ns are ALA-6, ILE-13, PHE-30, LEU-19, GLY-17, PHE-49, ALA-97, and LEU-4 in Figs. (**14a**, **b**). The LEU-4, LEU-19, LEU-27, TYR-29, PHE-30 and PHE-49 showed hydrophobic interactions. LEU-4 and ALA-97 showed backbone acceptor, while ALA-6 presented backbone donor hydrophobic interactions. On the other hand, the LEU-4, ALA-6, ILE-13, GLY-17, and ALA-97 residues showed bonding with the ligand by water-interacting hydrogen bonding. These interactions occurred more than 20% of the simulation time. During the simulation, the most interacting residues were ILE-13, with hydrogen bonding mediated by water molecules at 38% and hydrophobic interactions with PHE-30 in Figs. (**14b**, **e**). The MD analysis results also supported the results of the docking analysis, giving the residues of LEU-4, LEU-19, LEU-27, TYR-29, PHE-30 hydrophobic interactions and LEU-4, ALA-6, ILE-13, GLY-17, and ALA-97 residues water-interacting hydrogen bonding.

The MD analysis results also supported the results of the docking analysis, giving the residues of ILE-13, LEU-12, PHE-30, PHE-49, ASP-16, and THR-45 located in the binding region of DFR as residues interacting with the ligand. Combined, the docking and MD results reveal an intense match in key interaction residues and overall binding stability. However, the MD simulations offer a more detailed understanding by taking into account solvent effects and conformational flexibility. These findings confirm that terpinene-4-ol shows a robust and sustained binding profile against *Lactobacillus casei* DHFR, supporting its potential as a natural antibacterial agent targeting this microorganism. Overall, combining molecular docking and MD simulations provided a detailed understanding of how the structure of terpinene-4-ol affects its activity, highlighting its potential as a natural antimicrobial agent. These computational methods were crucial in pinpointing potential molecular targets, understanding how they bind, and providing predictive models for the development of anti-caries treatments based on plant chemicals.

According to Lipinski's rule of five, compounds with five or fewer hydrogen bond donors and 10 or fewer hydrogen bond acceptors are likely to achieve optimal oral bioavailability. ADME analysis of the terpinen-4-ol ligand showed (Table **6**) that these values are met. Since the molecular weights of the drug candidate compounds are below 500 Daltons, as per Lipinski's Rule of five, they are more easily and quickly absorbed and distributed throughout the body. The molecular weight of the terpinen-4-ol molecule is 154.25 g/mol. Overall, the molecular weights under 500 Daltons suggest a favourable potential for absorption by the body. LogP parameters determine how easily a drug candidate dissolves in fats. Its lipophilic properties allow it to pass through lipid-structured cell membranes with ease. The LogP value for the terpinen-4-ol molecule was found to be below 5. The skin permeability (Kp) parameter, which affects the transport of compounds through the mammalian epidermis, is determined by the lipophilic properties of the compound, specifically its molecular weight and the octanol/water partition coefficient. Furthermore, the varying polarities of the compounds impact skin absorption. Negative Log kp (-4.93 cm/s) values indicate the potential of the compounds to penetrate the skin.

CONCLUSION

In conclusion, TTO-NPs were successfully synthesized, which have spherical morphology with an average particle size of 221.6 nm, a PdI of 0.103, and a zeta potential of -5.22 mV. TTO-NPs presented a loading capacity of 25.65% and provided a biphasic extended release of TTO, which did not exceed the general oral exposure limits of TTO for 72 hours (total TTO release of 33.34 ± 2.17% after the first 5 h period and 97.61 ± 3.91% at the end of 72 h). *In vitro* safety and effectiveness studies showed that TTO-NPs were not mutagenic and had demonstrated good antimicrobial activity on various bacteria causing dental caries, such as *Streptococcus mutans*, *Lactobacillus casei*, *Lactobacillus acidophilus*, and *Scardovia wiggsiae*. Moreover, *in silico* studies supported the inhibitory effect of TTO on *Streptococcus mutans* and *Lactobacillus casei.* Since dental caries is a widespread oral disorder caused by the demineralization of tooth enamel due to acid production by bacteria, a long-lasting and effective antimicrobial dental care product will be beneficial to prevent dental caries. In recent years, researchers have focused on new formulations containing nanoparticles with great potential for dental caries prevention. In particular, the formulations containing essential oils with nano-sized and extended release properties provide superior reduction of biofilm accumulation and inhibition of bacteria that cause dental caries. It is worth mentioning that tea tree oil is widely used in oral hygiene. It is beneficial in treating halitosis by reducing both the bacterial load and the production of volatile sulphur compounds. Due to its low toxicity and natural origin, it is considered a phytomedicinal agent. TTO-NPs could be a promising formula, which is practically used either as a powder or mixed with 5-10 mL of water and applied to the mouth like a

mouthwash, providing a fresh mouth odour with effective inhibition of mouth pathogens and biofilm formation; it is noteworthy for further *in vivo* and clinical evaluations.

AUTHORS' CONTRIBUTIONS

The authors confirm their contribution to the paper as follows: YBK: supervision, project administration, data curation, conceptualization, writing- reviewing and editing. NC: Data curation, writing draft, project administration. SKG: data curation, conceptualization, writing-reviewing and editing. ŞS: data curation, writing-reviewing and editing, SAK: data curation, writing-reviewing and editing. PYA: conceptualization, writing, reviewing, EAY: conceptualization, data curation, conceptualization, writing-reviewing and editing, MK: Data curation, writing-reviewing and editing. All authors reviewed the results and approved the final version of the manuscript.

LIST OF ABBREVIATIONS

CT-DNA	=	Calf Thymus DNA
DCM	=	Dichloromethane
docking-MD	=	Molecular Docking
dynamics-MD	=	Molecular Dynamics
EDTA	=	Ethylenediaminetetraacetic Acid
EE	=	Encapsulation Efficiency
FTIR	=	Fourier Transform Infrared Spectroscopy
GC-FID	=	Gas Chromatography Coupled Flame Ionization Dedector
GC-FID/MS	=	Gas Chromatography Coupled with Flame Ionization Dedector/Mass Spectrometry
HCl	=	Hydrochloric Acid
LC	=	Loading Capacity
NaCl	=	Sodium Chloride
NaOH	=	Sodium Hydroxide
PLGA	=	Polylactic-co-glycolic Acid
PVA	=	Polyvinyl Alcohol
TEM	=	Transmission Electron Microscopy
TTO	=	Tea Tree Essential Oil
TTO-NPs	=	TTO-PLGA Nanoparticles

ETHICS APPROVAL AND CONSENT TO PARTICIPATE

Not applicable.

HUMAN AND ANIMAL RIGHTS

Not applicable.

CONSENT FOR PUBLICATION

Not applicable.

AVAILABILITY OF DATA AND MATERIALS

The data used to support the findings of this study are available from the researchers upon request.

FUNDING

This study was supported by TUBITAK Project (2209-A (1919B012004589)) titled "Production of Nanoformulation Containing Tea Tree Oil for Use in Prevention of Dental Caries and Investigation of Its *In vitro* Effectiveness".

CONFLICT OF INTEREST

The authors declare no conflict of interest, financial or otherwise.

ACKNOWLEDGEMENTS

In this study, the infrastructure of the Applied Nanotechnology and Antibody Production Laboratory established with TUBITAK support (project numbers: 115S132, 117S097 and 5200110) was used. The authors would also like to thank TUBITAK for their support. Authors are also very thankful to Schödinger's Drug Discovery Computational group for allowing us to use the docking program and Desmond MD program.

REFERENCES

[1] Şişko E, Dağhan Ş. What do the results of oral and dental health studies on school-age children in Turkey tell us?? J Cont Med Educ 2022; 31(1): 67-80.

[2] Banavar Ravi S, Nirupad S, Chippagiri P, Pandurangappa R. Antibacterial effects of natural herbal extracts on *Streptococcus mutans*: Can they be potential additives in dentifrices? Int J Dent 2017; 2017(1): 4921614.
PMID: 29201054

[3] Bader JD, Shugars DA, Bonito AJ. Systematic reviews of selected dental caries diagnostic and management methods. J Dent Educ 2001; 65(10): 960-8.
http://dx.doi.org/10.1002/j.0022-0337.2001.65.10.tb03470.x
PMID: 11699997

[4] Matalon S, Weiss EI, Gorfil C, Noy D, Slutzky H. *In vitro* antibacterial evaluation of flowable restorative materials. Quintessence Int 2009; 40(4): 327-32.
PMID: 19417878

[5] Çakır F, Gürgan S, Attar N. Caries microbiology. Hacettep Facult Dentistr J 2010; 34(3-4): 78-91.

[6] Hasslöf P, Stecksén-Blicks C. Probiotic Bacteria and Dental Caries. In: The Impact of Nutrition and Diet on Oral Health. Karger Publishers 2020; pp. 99-107.

[7] Qiu W, Zhou Y, Li Z, *et al.* Application of antibiotics/antimicrobial agents on dental caries. BioMed Res Int 2020; 2020(1): 5658212.
http://dx.doi.org/10.1155/2020/5658212 PMID: 32076608

[8] Chung JY, Choo JH, Lee MH, Hwang JK. Anticariogenic activity of macelignan isolated from *Myristica fragrans* (nutmeg) against *Streptococcus mutans*. Phytomedicine 2006; 13(4): 261-6.
http://dx.doi.org/10.1016/j.phymed.2004.04.007 PMID: 16492529

[9] Bassetti S, Tschudin-Sutter S, Egli A, Osthoff M. Optimizing antibiotic therapies to reduce the risk of bacterial resistance. Eur J Intern Med 2022; 99: 7-12.
http://dx.doi.org/10.1016/j.ejim.2022.01.029 PMID: 35074246

[10] Hemeg H. Nanomaterials for alternative antibacterial therapy. Int J Nanomed 2017; 12: 8211-25.
http://dx.doi.org/10.2147/IJN.S132163 PMID: 29184409

[11] Allaker RP, Memarzadeh K. Nanoparticles and the control of oral infections. Int J Antimicrob Agents 2014; 43(2): 95-104.
http://dx.doi.org/10.1016/j.ijantimicag.2013.11.002 PMID: 24388116

[12] Shrestha A, Zhilong S, Gee NK, Kishen A. Nanoparticulates for antibiofilm treatment and effect of aging on its antibacterial activity. J Endod 2010; 36(6): 1030-5.
http://dx.doi.org/10.1016/j.joen.2010.02.008 PMID: 20478460

[13] Besinis A, De Peralta T, Tredwin CJ, Handy RD. Review of nanomaterials in dentistry: Interactions with the oral microenvironment, clinical applications, hazards, and benefits. ACS Nano 2015; 9(3): 2255-89.
http://dx.doi.org/10.1021/nn505015e PMID: 25625290

[14] Yazdanian M, Motallaei MN, Tahmasebi E, *et al.* Chemical characterization and cytotoxic/antibacterial effects of nine Iranian propolis extracts on human fibroblast cells and oral bacteria. BioMed Res Int 2022; 2022(1): 6574997.
http://dx.doi.org/10.1155/2022/6574997 PMID: 35434137

[15] Moghadam ET, Yazdanian M, Alam M. Current natural bioactive materials in bone and tooth regeneration in dentistry: A comprehensive overview. JMR&T 2021; 13: 2078-114.
[16] Hannig M, Hannig C. Nanomaterials in preventive dentistry. Nat Nanotechnol 2010; 5(8): 565-9. http://dx.doi.org/10.1038/nnano.2010.83 PMID: 20581832
[17] Cheng L, Zhang K, Weir MD, Melo MAS, Zhou X, Xu HHK. Nanotechnology strategies for antibacterial and remineralizing composites and adhesives to tackle dental caries. Nanomedicine (Lond) 2015; 10(4): 627-41. http://dx.doi.org/10.2217/nnm.14.191 PMID: 25723095
[18] Worthington RJ, Richards JJ, Melander C. Small molecule control of bacterial biofilms. Org Biomol Chem 2012; 10(37): 7457-74. http://dx.doi.org/10.1039/c2ob25835h PMID: 22733439
[19] Rabin N, Zheng Y, Opoku-Temeng C, Du Y, Bonsu E, Sintim HO. Agents that inhibit bacterial biofilm formation. Future Med Chem 2015; 7(5): 647-71. http://dx.doi.org/10.4155/fmc.15.7 PMID: 25921403
[20] Jeon JG, Rosalen PL, Falsetta ML, Koo H. Natural products in caries research: Current (limited) knowledge, challenges and future perspective. Caries Res 2011; 45(3): 243-63. http://dx.doi.org/10.1159/000327250 PMID: 21576957
[21] Chitme HR, Chandra M, Kaushik S. Studies on anti-diarrhoeal activity of *Calotropis gigantea* R.Br. in experimental animals. J Pharm Pharm Sci 2004; 7(1): 70-5. PMID: 15144737
[22] Çakır NT, Kaleağası S, Kökdil G. Tea tree oil: As a promising antimicrobial agent. J Fac Pharm Ankara 2005; 34(4): 315-27.
[23] Hammer KA, Carson CF, Riley TV, Nielsen JB. A review of the toxicity of *Melaleuca alternifolia* (tea tree) oil. Food Chem Toxicol 2006; 44(5): 616-25. http://dx.doi.org/10.1016/j.fct.2005.09.001 PMID: 16243420
[24] Kairey L, Agnew T, Bowles EJ, Barkla BJ, Wardle J, Lauche R. Efficacy and safety of *Melaleuca alternifolia* (tea tree) oil for human health: A systematic review of randomized controlled trials. Front Pharmacol 2023; 14: 1116077. http://dx.doi.org/10.3389/fphar.2023.1116077 PMID: 37033604
[25] Mohammed AE, Aldahasi RM, Rahman I, *et al.* The antimicrobial activity of tea tree oil (*Melaleuca alternifolia*) and its metal nanoparticles in oral bacteria. PeerJ 2024; 12: e17241. http://dx.doi.org/10.7717/peerj.17241 PMID: 38854801
[26] Madene A, Jacquot M, Scher J. Flavour encapsulation and controlled release: A review. IJFST 2006; 41(1): 1-21.
[27] Shahidi F, Han XQ. Encapsulation of food ingredients. Crit Rev Food Sci Nutr 1993; 33(6): 501-47. http://dx.doi.org/10.1080/10408399309527645 PMID: 8216812
[28] Turasan H, Sahin S, Sumnu G. Encapsulation of rosemary essential oil. Lebensm Wiss Technol 2015; 64(1): 112-9. http://dx.doi.org/10.1016/j.lwt.2015.05.036
[29] Asbahani AE, Miladi K, Badri W, *et al.* Essential oils: From extraction to encapsulation. Int J Pharm 2015; 483(1-2): 220-43. http://dx.doi.org/10.1016/j.ijpharm.2014.12.069 PMID: 25683145
[30] Li M, Zhu L, Liu B, *et al.* Tea tree oil nanoemulsions for inhalation therapies of bacterial and fungal pneumonia. Colloids Surf B Biointerfaces 2016; 141: 408-16. http://dx.doi.org/10.1016/j.colsurfb.2016.02.017 PMID: 26895502
[31] Abdollahi S, Lotfipour F. PLGA-and PLA-based polymeric nanoparticles for antimicrobial drug delivery. Biomed Int 2012; 3(1): 1-11.
[32] Ercin E, Kecel-Gunduz S, Gok B, Aydin T, Budama-Kilinc Y, Kartal M. *Laurus nobilis L.* essential oil-loaded PLGA as a nanoformulation candidate for cancer treatment. Molecules 2022; 27(6): 1899. http://dx.doi.org/10.3390/molecules27061899 PMID: 35335262
[33] Egil AC, Ozdemir B, Gok B, Kecel-Gunduz S, Budama-Kilinc Y. Synthesis, characterization, biological activities and molecular docking of Epilobium parviflorum aqueous extract loaded chitosan nanoparticles. Int J Biol Macromol 2020; 161: 947-57. http://dx.doi.org/10.1016/j.ijbiomac.2020.06.066 PMID: 32544580
[34] Budama-Kilinc Y, Kecel-Gunduz S, Ozdemir B, *et al.* New nanodrug design for cancer therapy: Its synthesis, formulation, *in vitro* and *in silico* evaluations. Arch Pharm (Weinheim) 2020; 353(11): 2000137. http://dx.doi.org/10.1002/ardp.202000137 PMID: 32757360
[35] Sarwar T, Ishqi HM, Rehman SU, Husain MA, Rahman Y, Tabish M. Caffeic acid binds to the minor groove of calf thymus DNA: A multi-spectroscopic, thermodynamics and molecular modelling study. Int J Biol Macromol 2017; 98: 319-28. http://dx.doi.org/10.1016/j.ijbiomac.2017.02.014 PMID: 28167108
[36] Dantas FGS, Castilho PF, Almeida-Apolonio AA, Araújo RP, Oliveira KMP. Mutagenic potential of medicinal plants evaluated by the Ames Salmonella/microsome assay: A systematic review. Mutat Res Rev Mutat Res 2020; 786: 108338. http://dx.doi.org/10.1016/j.mrrev.2020.108338 PMID: 33339578
[37] Compound Summary for CID 11230, 4-Carvomenthenol. Available from: Carvomenthenol.https://pubchem.ncbi.nlm.nih.gov/compound/4-Carvomenthenol.
[38] Ito K, Ito S, Shimamura T, *et al.* Crystal structure of glucansucrase from the dental caries pathogen *Streptococcus mutans*. J Mol Biol 2011; 408(2): 177-86. http://dx.doi.org/10.1016/j.jmb.2011.02.028 PMID: 21354427
[39] Polshakov VI, Birdsall B, Frenkiel TA, Gargaro AR, Feeney J. Structure and dynamics in solution of the complex of *lactobacillus casei* dihydrofolate reductase with the new lipophilic antifolate drug trimetrexate. Protein Sci 1999; 8(3): 467-81. http://dx.doi.org/10.1110/ps.8.3.467 PMID: 10091649
[40] Burley SK, Bhikadiya C, Bi C, *et al.* RCSB Protein Data bank: Powerful new tools for exploring 3D structures of biological macromolecules for basic and applied research and education in fundamental biology, biomedicine, biotechnology, bioengineering and energy sciences. Nucleic Acids Res 2021; 49(D1): D437-51. http://dx.doi.org/10.1093/nar/gkaa1038 PMID: 33211854
[41] Friesner RA, Banks JL, Murphy RB, *et al.* Glide: a new approach for rapid, accurate docking and scoring. 1. Method and assessment of docking accuracy. J Med Chem 2004; 47(7): 1739-49. http://dx.doi.org/10.1021/jm0306430 PMID: 15027865
[42] Friesner RA, Murphy RB, Repasky MP, *et al.* Extra precision glide: Docking and scoring incorporating a model of hydrophobic enclosure for protein-ligand complexes. J Med Chem 2006; 49(21): 6177-96. http://dx.doi.org/10.1021/jm051256o PMID: 17034125
[43] Olsson MHM, Søndergaard CR, Rostkowski M, Jensen JH. PROPKA3: Consistent treatment of internal and surface residues in empirical p K a predictions. J Chem Theory Comput 2011; 7(2): 525-37. http://dx.doi.org/10.1021/ct100578z PMID: 26596171
[44] Harder E, Damm W, Maple J, *et al.* OPLS3: A force field providing broad coverage of drug-like small molecules and proteins. J Chem Theory Comput 2016; 12(1): 281-96. http://dx.doi.org/10.1021/acs.jctc.5b00864 PMID: 26584231
[45] Release S. 1: Desmond Molecular Dynamics System. In: Maestro-Desmond Interoperability Tools. New York, NY: Schrödinger 2019.
[46] Release S. 3: Desmond molecular dynamics system. In: Maestro-Desmond Interoperability Tools. Schrödinger 2017.
[47] Ge Y, Ge M. Distribution of *Melaleuca alternifolia* essential oil in liposomes with Tween 80 addition and enhancement of *in vitro* antimicrobial effect. J Exp Nanosci 2016; 11(5): 345-58. http://dx.doi.org/10.1080/17458080.2015.1065013
[48] Thiagarajan P, Banerjee K, Saha G. Alumina nanoparticle incorporated *Melaleuca alternifolia* oil formulation for control of *Streptococcus mutans* isolated from dental caries. J Microbiol Biotechnol Food Sci 2019; 9(1): 44-52. http://dx.doi.org/10.15414/jmbfs.2019.9.1.44-52
[49] Sharma D, Maheshwari D, Philip G, *et al.* Formulation and optimization of polymeric nanoparticles for intranasal delivery of lorazepam using Box-Behnken design: *In vitro* and *in vivo* evaluation. BioMed Res Int 2014; 2014(1): 156010. PMID: 25126544
[50] Alhobeira HA, Al Mogbel M, Khan S, *et al.* Prioritization and characterization of validated biofilm blockers targeting glucosyltransferase C of *Streptococcus mutans*. Artif Cells Nanomed Biotechnol 2021; 49(1): 335-44. http://dx.doi.org/10.1080/21691401.2021.1903021 PMID: 33783274

[51] Zu S, Chen T, Li S. Global optimization-based inference of chemogenomic features from drug-target interactions. Bioinformatics 2015; 31(15): 2523-9. http://dx.doi.org/10.1093/bioinformatics/btv181 PMID: 25819672

[52] Hobani Y, Jerah A, Bidwai A. A comparative molecular docking study of curcumin and methotrexate to dihydrofolate reductase. Bioinformation 2017; 13(3): 63-6. http://dx.doi.org/10.6026/97320630013063 PMID: 28584445

[53] Warhurst DC. Antimalarial drug discovery: Development of inhibitors of dihydrofolate reductase active in drug resistance. Drug Discov Today 1998; 3(12): 538-46. http://dx.doi.org/10.1016/S1359-6446(98)01268-9

[54] Wang L, Hu C, Shao L. The antimicrobial activity of nanoparticles: Present situation and prospects for the future. Int J Nanomedicine 2017; 12: 1227-49. http://dx.doi.org/10.2147/IJN.S121956 PMID: 28243086

[55] Aflakian F, Mirzavi F, Aiyelabegan HT, *et al.* Nanoparticles-based therapeutics for the management of bacterial infections: A special emphasis on FDA approved products and clinical trials. Eur J Pharm Sci 2023; 188: 106515. http://dx.doi.org/10.1016/j.ejps.2023.106515 PMID: 37402428

[56] Mondal SK, Chakraborty S, Manna S, Mandal SM. Antimicrobial nanoparticles: Current landscape and future challenges. RSC Pharmaceutics 2024; 1(3): 388-402. http://dx.doi.org/10.1039/D4PM00032C

[57] Priyadarshini BM, Antipina MN, Fawzy AS. Formulation and characterisation of poly(lactic-co-glycolic acid) encapsulated clove oil nanoparticles for dental applications. IET Nanobiotechnol 2018; 12(3): 311-7. http://dx.doi.org/10.1049/iet-nbt.2017.0141

[58] Phuangkaew T, Booranabunyat N, Kiatkamjornwong S, Thanyasrisung P, Hoven VP. Amphiphilic quaternized chitosan: Synthesis, characterization, and anti-cariogenic biofilm property. Carbohydr Polym 2022; 277: 118882. http://dx.doi.org/10.1016/j.carbpol.2021.118882 PMID: 34893285

[59] Ferreira IJ, de Menezes LR, Tavares MIB. Morphological and structural evaluation of nanoparticles loaded with tea tree oil for the therapeutic treatment of HPV. Polym Bull 2022; 79(7): 5457-79. http://dx.doi.org/10.1007/s00289-021-03780-0

[60] Minhaco VMTR, Maquera Huacho PM, Mancim Imbriani MJ, *et al.* Improving antimicrobial activity against endodontic biofilm after exposure to blue light-activated novel curcumin nanoparticle. Photodiagn Photodyn Ther 2023; 42: 103322. http://dx.doi.org/10.1016/j.pdpdt.2023.103322 PMID: 36773754

[61] Budama-Kilinc Y, Kurtur OB, Gok B, *et al.* Production of prophylactic nanoformulation for dental caries and investigation of its effectiveness by *in vitro* and *in silico* methods. Pharmaceutics 2025; 17(2): 167. http://dx.doi.org/10.3390/pharmaceutics17020167 PMID: 40006534

[62] Mainardes RM, Evangelista RC. PLGA nanoparticles containing praziquantel: Effect of formulation variables on size distribution. Int J Pharm 2005; 290(1-2): 137-44. http://dx.doi.org/10.1016/j.ijpharm.2004.11.027 PMID: 15664139

[63] Danaei M, Dehghankhold M, Ataei S, *et al.* Impact of particle size and polydispersity index on the clinical applications of lipidic nanocarrier systems. Pharmaceutics 2018; 10(2): 57. http://dx.doi.org/10.3390/pharmaceutics10020057 PMID: 29783687

[64] Frickenstein AN, Mukherjee S, Harcourt T, *et al.* Quantification of monodisperse and biocompatible gold nanoparticles by single-particle ICP-MS. Anal Bioanal Chem 2023; 415(18): 4353-66. http://dx.doi.org/10.1007/s00216-023-04540-x PMID: 36670192

[65] Budama-Kilinc Y. Piperine nanoparticles for topical application: Preparation, characterization, *in vitro* and *in silico* evaluation. ChemistrySelect 2019; 4(40): 11693-700. http://dx.doi.org/10.1002/slct.201903266

[66] Panyam J, Williams D, Dash A, Leslie-Pelecky D, Labhasetwar V. Solid-state solubility influences encapsulation and release of hydrophobic drugs from PLGA/PLA nanoparticles. J Pharm Sci 2004; 93(7): 1804-14. http://dx.doi.org/10.1002/jps.20094 PMID: 15176068

[67] Esfandyari-Manesh M, Ghaedi Z, Asemi M, *et al.* Study of antimicrobial activity of anethole and carvone loaded PLGA nanoparticles. J Pharm Res 2013; 7(4): 290-5. http://dx.doi.org/10.1016/j.jopr.2013.04.019

[68] Almeida KB, Araujo JL, Cavalcanti JF, *et al. In vitro* release and anti-herpetic activity of *Cymbopogon citratus* volatile oil-loaded nanogel. Rev Bras Farmacogn 2018; 28(4): 495-502. http://dx.doi.org/10.1016/j.bjp.2018.05.007

[69] Kumar S, Sangwan P, Lather V, Pandita D. Biocompatible PLGA-oil hybrid nanoparticles for high loading and controlled delivery of resveratrol. J Drug Deliv Sci Technol 2015; 30: 54-62. http://dx.doi.org/10.1016/j.jddst.2015.09.016

[70] Mokhtareeizadeh Z, Homayouni Tabrizi M. Optimisation of *Ferula assa-foetida* -Loaded PLGA Nanoparticles Synthesised and evaluation of putative mechanism for anticancer properties. Mater Technol 2022; 37(11): 1954-67. http://dx.doi.org/10.1080/10667857.2021.2016293

[71] Li D. Encyclopedia of microfluidics and nanofluidics. Springer Science & Business Media 2008. http://dx.doi.org/10.1007/978-0-387-48998-8

[72] Gursu BY, Dag İ, Dikmen G. Antifungal and antibiofilm efficacy of cinnamaldehyde-loaded poly(DL-lactide-co-glycolide) (PLGA) nanoparticles against *Candida albicans*. Int Microbiol 2022; 25(2): 245-58. http://dx.doi.org/10.1007/s10123-021-00210-z PMID: 34528147

[73] Khan I, Joshi G, Nakhate KT, Ajazuddin , Kumar R, Gupta U. Nano-co-delivery of berberine and anticancer drug using PLGA nanoparticles: exploration of better anticancer activity and *in vivo* kinetics. Pharm Res 2019; 36(10): 149. http://dx.doi.org/10.1007/s11095-019-2677-5 PMID: 31420752

[74] Vishwakarma GS, Gautam N, Babu JN, Mittal S, Jaitak V. Polymeric encapsulates of essential oils and their constituents: A review of preparation techniques, characterization, and sustainable release mechanisms. Polym Rev (Phila Pa) 2016; 56(4): 668-701. http://dx.doi.org/10.1080/15583724.2015.1123725

[75] Lammari N, Louaer O, Meniai AH, Elaissari A. Encapsulation of essential oils *via* nanoprecipitation process: Overview, progress, challenges and prospects. Pharmaceutics 2020; 12(5): 431. http://dx.doi.org/10.3390/pharmaceutics12050431 PMID: 32392726

[76] Yang FL, Li XG, Zhu F, Lei CL. Structural characterization of nanoparticles loaded with garlic essential oil and their insecticidal activity against *Tribolium castaneum* (Herbst) (Coleoptera: Tenebrionidae). J Agric Food Chem 2009; 57(21): 10156-62. http://dx.doi.org/10.1021/jf9023118 PMID: 19835357

[77] Rytwo G, Zakai R, Wicklein B. The use of ATR-FTIR spectroscopy for quantification of adsorbed compounds. J Spectrosc 2015; 2015(1): 1-8. http://dx.doi.org/10.1155/2015/727595

[78] Ocak B, Gülümser G, Baloğlu E. Microencapsulation of *Melaleuca alternifolia* (tea tree) oil by using simple coacervation method. J Essent Oil Res 2011; 23(4): 58-65. http://dx.doi.org/10.1080/10412905.2011.9700470

[79] Kaur J, Singh RR, Khan E, Kumar A, Joshi A. Piperine-loaded PLGA nanoparticles as cancer drug carriers. ACS Appl Nano Mater 2021; 4(12): 14197-207. http://dx.doi.org/10.1021/acsanm.1c03664

[80] Pakravan P, Masoudian S. Study on the interaction between isatin-β-thiosemicarbazone and calf thymus DNA by spectroscopic techniques. Iran J Pharm Res 2015; 14(1): 111-23. PMID: 25561917

[81] Salehi F, Jamali T, Kavoosi G, Ardestani SK, Vahdati SN. Stabilization of Zataria essential oil with pectin-based nanoemulsion for enhanced cytotoxicity in monolayer and spheroid drug-resistant breast cancer cell cultures and deciphering its binding mode with gDNA. Int J Biol Macromol 2020; 164: 3645-55. http://dx.doi.org/10.1016/j.ijbiomac.2020.08.084 PMID: 32795576

[82] Liu T, Kang J, Liu L. Thymol as a critical component of *Thymus vulgaris L.* essential oil combats *Pseudomonas aeruginosa* by intercalating DNA and inactivating biofilm. Lebensm Wiss Technol 2021; 136: 110354. http://dx.doi.org/10.1016/j.lwt.2020.110354

[83] Evandri MG, Battinelli L, Daniele C, Mastrangelo S, Bolle P, Mazzanti G. The antimutagenic activity of *Lavandula angustifolia*> (lavender) essential oil in the bacterial reverse mutation assay. Food Chem Toxicol 2005; 43(9): 1381-7.

http://dx.doi.org/10.1016/j.fct.2005.03.013 PMID: 15907354

[84] Ruiz-Pérez NJ, González-Ávila M, Sánchez-Navarrete J, *et al.* Antimycotic activity and genotoxic evaluation of *Citrus sinensis and Citrus latifolia* essential oils. Sci Rep 2016; 6(1): 25371. http://dx.doi.org/10.1038/srep25371 PMID: 27137128

[85] Nalini T, Basha SK, Sadiq AM, Kumari VS. *In vitro* cytocompatibility assessment and antibacterial effects of quercetin encapsulated alginate/chitosan nanoparticle. Int J Biol Macromol 2022; 219: 304-11. http://dx.doi.org/10.1016/j.ijbiomac.2022.08.007 PMID: 35934075

[86] Christopoulou SD, Androutsopoulou C, Hahalis P, Kotsalou C, Vantarakis A, Lamari FN. Rosemary extract and essential oil as drink ingredients: An evaluation of their chemical composition, genotoxicity, antimicrobial, antiviral, and antioxidant properties. Foods 2021; 10(12): 3143. http://dx.doi.org/10.3390/foods10123143 PMID: 34945695

[87] Li WR, Li HL, Shi QS, *et al.* The dynamics and mechanism of the antimicrobial activity of tea tree oil against bacteria and fungi. Appl Microbiol Biotechnol 2016; 100(20): 8865-75. http://dx.doi.org/10.1007/s00253-016-7692-4 PMID: 27388769

[88] Mortelmans K, Zeiger E. The Ames Salmonella/microsome mutagenicity assay. Mutat Res 2000; 455(1-2): 29-60. http://dx.doi.org/10.1016/S0027-5107(00)00064-6 PMID: 11113466

[89] Shoeibi S, Rahimifard N, Pirouz B. Mutagenicity of four natural flavors: Clove, cinnamon, thyme and *Zataria multiflora* boiss. Faslnamah-i Giyahan-i Daruyi 2009; 8(29): 89-96.

[90] Casalle N, de Andrade CR. Cytotoxic and mutagenic capacity of TTO and terpinen-4-ol in oral squamous cell carcinoma. BioRxiv 2020; 2020.01.

[91] Chávez-Magdaleno ME, Luque-Alcaraz A, Gutiérrez-Martínez P. Effect of chitosan-pepper tree (*Schinus molle*) essential oil biocomposites on the growth kinetics, viability and membrane integrity of colletotrichum gloeosporioides. Rev Mex Ing Quim 2017; 17(1): 29-45. http://dx.doi.org/10.24275/uam/izt/dcbi/revmexingquim/2018v17n1/Chavez

[92] Kapustová M, Puškárová A, Bučková M, *et al.* Biofilm inhibition by biocompatible poly(ε-caprolactone) nanocapsules loaded with essential oils and their cyto/genotoxicity to human keratinocyte cell line. Int J Pharm 2021; 606: 120846. http://dx.doi.org/10.1016/j.ijpharm.2021.120846 PMID: 34216769

[93] Borodina N, Raal A, Kovalyov V, *et al.* Phytochemical research and antimicrobial properties of lipophylic extracts of some species of Salix L. genus from Ukraine. Open Agric J 2020; 14(1): 136-44. http://dx.doi.org/10.2174/1874331502014010136

[94] Downes J, Mantzourani M, Beighton D, *et al. Scardovia wiggsiae sp.* nov., isolated from the human oral cavity and clinical material, and emended descriptions of the genus Scardovia and *Scardovia inopinata.* Int J Syst Evol Microbiol 2011; 61(1): 25-9. http://dx.doi.org/10.1099/ijs.0.019752-0 PMID: 20139283

[95] Jeong SJ. Effects of *Lactobacillus casei* and *Aggregatibactor actinomycetemcomitans* against *Streptococcus mutans* according to the concentration of sucrose. J Dental Hygiene Sci 2023; 23(2): 103-11. http://dx.doi.org/10.17135/jdhs.2023.23.2.103

[96] Ikuma K, Decho AW, Lau BLT. When nanoparticles meet biofilms-interactions guiding the environmental fate and accumulation of nanoparticles. Front Microbiol 2015; 6: 591. http://dx.doi.org/10.3389/fmicb.2015.00591 PMID: 26136732

[97] Moradialvand M, Asri N, Jahdkaran M, Beladi M, Houri H. Advancements in nanoparticle-based strategies for enhanced antibacterial interventions. Cell Biochem Biophys 2024; 82(4): 3071-90. http://dx.doi.org/10.1007/s12013-024-01428-0 PMID: 39023679

[98] Amissah F, Andey T, Ahlschwede KM. Nanotechnology-based therapies for the prevention and treatment of *Streptococcus mutans*-derived dental caries. J Oral Biosci/JAOB, Jpn Assoc Oral Biol 2021; 63(4): 327-36. http://dx.doi.org/10.1016/j.job.2021.09.002 PMID: 34536629

[99] Zhu T, Huang Z, Shu X. Functional nanomaterials and their potentials in antibacterial treatment of dental caries. Colloid Surfaces B Biointerf 2022; 218: 112761. http://dx.doi.org/10.1016/j.colsurfb.2022.112761

[100] Yasin M, Younis A, Javed T, *et al.* River tea tree oil: Composition, antimicrobial and antioxidant activities, and potential applications in agriculture. Plants 2021; 10(10): 2105. http://dx.doi.org/10.3390/plants10102105 PMID: 34685914

[101] Brun P, Bernabè G, Filippini R, Piovan A. *In vitro* antimicrobial activities of commercially available tea tree (*Melaleuca alternifolia*) essential oils. Curr Microbiol 2019; 76(1): 108-16. http://dx.doi.org/10.1007/s00284-018-1594-x PMID: 30421144

[102] Kanth MR, PRAKASH A, Sreenath G. Efficacy of specific plant products on dental caries causing microorganisms. JCDR 2016; 10(12)

[103] Koh KJ, Pearce AL, Marshman G, Finlay-Jones JJ, Hart PH. Tea tree oil reduces histamine-induced skin inflammation. Br J Dermatol 2002; 147(6): 1212-7. http://dx.doi.org/10.1046/j.1365-2133.2002.05034.x PMID: 12452873

[104] Pazyar N, Yaghoobi R, Bagherani N, Kazerouni A. A review of applications of tea tree oil in dermatology. Int J Dermatol 2013; 52(7): 784-90. http://dx.doi.org/10.1111/j.1365-4632.2012.05654.x PMID: 22998411

[105] Carson CF, Hammer KA, Riley TV. *Melaleuca alternifolia* (Tea Tree) oil: A review of antimicrobial and other medicinal properties. Clin Microbiol Rev 2006; 19(1): 50-62. http://dx.doi.org/10.1128/CMR.19.1.50-62.2006 PMID: 16418522

[106] Yallapu MM, Gupta BK, Jaggi M, Chauhan SC. Fabrication of curcumin encapsulated PLGA nanoparticles for improved therapeutic effects in metastatic cancer cells. J Colloid Interface Sci 2010; 351(1): 19-29. http://dx.doi.org/10.1016/j.jcis.2010.05.022 PMID: 20627257

[107] Fydrych D, Jeziurska J, Wełna J, Kwiecińska-Piróg J. Potential use of selected natural compounds with Anti-Biofilm activity. Int J Mol Sci 2025; 26(2): 607. http://dx.doi.org/10.3390/ijms26020607 PMID: 39859320

[108] Horev B, Klein MI, Hwang G, *et al.* pH-activated nanoparticles for controlled topical delivery of farnesol to disrupt oral biofilm virulence. ACS Nano 2015; 9(3): 2390-404. http://dx.doi.org/10.1021/nn507170s PMID: 25661192

[109] da Silva DR, Deps TD, Sakaguchi OAS. Molecular docking of phytochemicals against *Streptococcus mutans* virulence targets: A proteomic insight into drug planning. In: Oral Health Care-An Important Issue of the Modern Society. IntechOpen 2022.

[110] Dams T, Auerbach G, Bader G, *et al.* The crystal structure of dihydrofolate reductase from *Thermotoga maritima*: molecular features of thermostability. J Mol Biol 2000; 297(3): 659-72. http://dx.doi.org/10.1006/jmbi.2000.3570 PMID: 10731419

[111] Zhang Q, Nguyen T, McMichael M, *et al.* New small-molecule inhibitors of dihydrofolate reductase inhibit *Streptococcus mutans*. Int J Antimicrob Agents 2015; 46(2): 174-82. http://dx.doi.org/10.1016/j.ijantimicag.2015.03.015 PMID: 26022931

[112] Polshakov VI. Dihydrofolate reductase: Structural aspects of mechanisms of enzyme catalysis and inhibition. Russ Chem Bull 2001; 50(10): 1733-51. http://dx.doi.org/10.1023/A:1014313625350